CHALMERS

Investigation of Dynamic Friction Properties of a Dual Mass Flywheel for Commercial Vehicles

Master's thesis in Automotive Engineering

JOHAN KARLSSON

Department of Mechanics and Maritime Sciences
CHALMERS UNIVERSITY OF TECHNOLOGY
Göteborg, Sweden 2018

MASTER'S THESIS IN AUTOMOTIVE ENGINEERING

Investigation of Dynamic Friction Properties of a Dual Mass Flywheel for Commercial Vehicles

JOHAN KARLSSON

Department of Mechanics and Maritime Sciences
Division of Dynamics
CHALMERS UNIVERSITY OF TECHNOLOGY

Göteborg, Sweden 2018

Investigation of Dynamic Friction Properties of a Dual Mass Flywheel for Commercial Vehicles
JOHAN KARLSSON

Master's thesis 2018:19
Department of Mechanics and Maritime Sciences
Division of Dynamics
Chalmers University of Technology
SE-412 96 Göteborg
Sweden
Telephone: +46 (0)31-772 1000

Cover:
A Volvo FH16 truck and a dual mass flywheel mounted to a 16 l Volvo engine [1].

Chalmers Reproservice
Göteborg, Sweden 2018

Investigation of Dynamic Friction Properties of a Dual Mass Flywheel for Commercial Vehicles
Master's thesis in Automotive Engineering
JOHAN KARLSSON
Department of Mechanics and Maritime Sciences
Division of Dynamics
Chalmers University of Technology

Abstract

In order to meet new requirements on exhaust emissions the trend is to downsize and reduce the speed of conventional engines. This leads to larger vibrations levels transmitted to the rest of the powertrain and ultimately to the rest of the vehicle. One way of reducing the transmission of these vibrations is to use a dual mass flywheel. This is a common solution for passenger cars but not as well known for commercial vehicles.

In this master thesis the dynamic friction properties of a dual mass flywheel for a heavy duty truck is analysed. The analysis involves both simulations and physical experiments. The aim is to investigate how the friction is depending on rotational speed and torque and how well the simulation model correlates with the measured values.

The simulations were done in MATLAB with a linear spring damper model. The input to the model was a torque signal and the final output was the dynamic behaviour of the dual mass flywheel. The friction losses were then determined by analysing the input torque and the resulting movement of the dual mass flywheel.

A test rig at AB Volvo's site in Lundby was used for the measurements. A dual mass flywheel for a Volvo FH16 truck was rotated at different speed with different levels of torque amplitude. The speeds of the primary and secondary masses of the flywheel were measured along with the torque input to the system. The friction losses were then calculated by analysing the measured torque and movement of the dual mass flywheel.

The results from the measurements indicate that the friction in the dual mass flywheel is primarily viscous. This means that the losses are dependent on the speed difference between the primary and secondary mass. No direct relation between the losses and the rotational speed could be found. The results show the same behaviour when the linear simulation model is used to calculate the losses. If the right value of the damping coefficient is used the results from the measurements and the simulations are similar.

Keywords: Dual Mass Flywheel, DMF, Torsional Vibrations, Commercial Vehicles

Acknowledgements

Firstly I would like to thank my supervisors Lina Wramner and Anders Hedman for their continuous support and guidance throughout the project. I also want to express my gratitude to Johan Jonsson at AB Volvo for his great support within the measurement part of the project. A sincere thanks also to my examiner Viktor Berbyuk for his supervision and guidance.

Furthermore I want to give a special thanks to all employees at AB Volvo that have been involved within the project. Both the personnel in the transmission and electric workshop and the engineers involved. In the workshop I would especially like to thank Christer Doverhag for all the mechanical work he has put in to the project. Last but not least I would like to thank AB Volvo who has financed the project and made it possible.

Johan Karlsson, Göteborg, May 2018

Contents

1 Introduction

1.1 Background

There is currently a trend within the vehicle industry to downsize and reduce the speed of conventional engines. This is done in order to reduce emissions and is done for both passenger cars and heavy vehicles. However, maintaining the same output power will increase the torsional vibrations generated. They will be transmitted to the rest of the powertrain and ultimately to the driver and passenger compartment. One way of reducing the transmission of these vibrations is to use a dual mass flywheel (DMF). This is common for passenger cars but is seldom used for heavy vehicles. If DMFs are to be used to a larger extent in heavy vehicles it is important to understand the dynamic properties of the product. This master thesis aims at better understanding the friction properties of a DMF for heavy trucks.

1.2 Aim

The aim of the project is to develop linear simulation models for DMFs and perform physical experiments to measure the friction losses in the DMF. By analysing and comparing the results the parameters of the model should be correlated to the measurement data. Finally it should be investigated in which areas a linear simulation model gives results that are similar to the measured experimental data.

1.3 Limitations

The project is to be performed during 20 weeks. To be able to deliver results within this deadline the following limitations are set.

- The main focus is second order engine vibrations and constant engine speed, both in the simulations and in the experiments.
- The thesis will not investigate other means of reducing vibrations from the engine, neither will it concern how the remaining torsional vibrations are affecting the vehicle downstream of the flywheel.
- Test rigs and equipment at AB Volvo will be used for the measurements.
- Experiments will be performed with DMFs provided by AB Volvo.

1.4 Specification of issue under investigation

There are two major questions that should be answered at the end of this master thesis.

- How is the friction in the DMF depending on input speed and torque?
- How well can this be predicted with a linear simulation model?

2 Theory

2.1 Torsional vibrations in the powertrain

The torsional vibrations in the powertrain originate from the uneven torque and power output from the engine. A four stroke single cylinder engine fires every 720 crank angle degree (CAD). This causes fluctuations in output torque and output speed. If more cylinders are added to form for example an inline six cylinder engine the firing interval becomes 120 CAD. The fluctuations in torque and speed for this engine are reduced but far from eliminated [2]. These fluctuations in torque are the reason a flywheel or something similar is used on all vehicles with internal combustion engines. A conventional flywheel is a large disc in metal that is located between the crankshaft and the clutch. The inertia of the flywheel evens out the fluctuations in torque and speed from the engine. A plot of the torque fluctuations from an inline six cylinder engine at 1200 rpm and the resulting torque fluctuations at the flywheel can be seen in Figure 2.1.

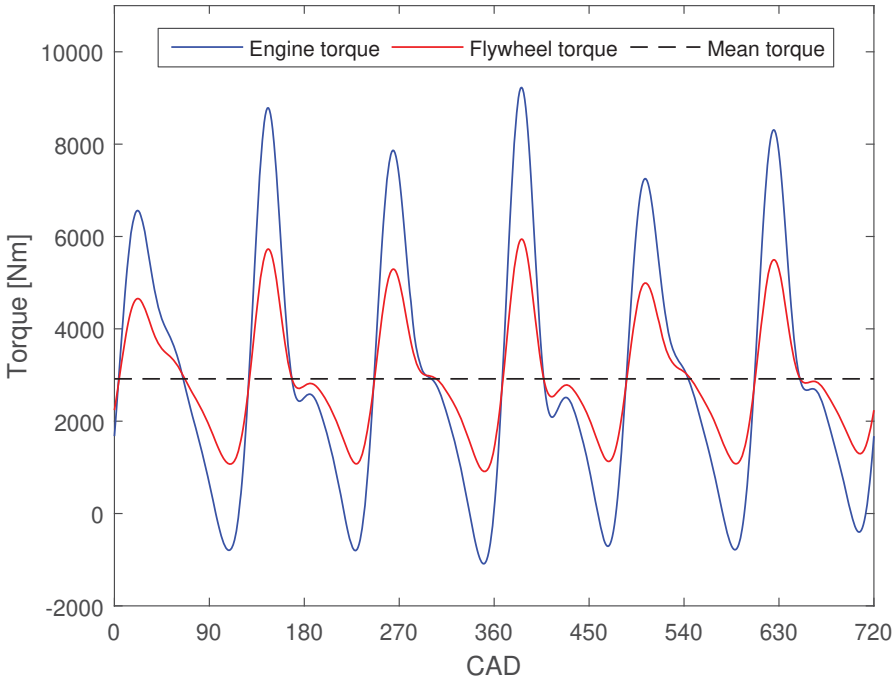

Figure 2.1: *Torque fluctuation from the engine and at the flywheel.*

2.2 Dual mass flywheel

A dual mass flywheel can be used when a conventional single mass flywheel does not sufficiently dampen the torsional vibrations from the engine. A DMF acts as a low pass filter for the torque and speed transmitted to the rest of the drive train [3]. As can be understood from the name a DMF consists of two masses. The primary mass (also called primary flywheel) is bolted to the crankshaft, just like a conventional flywheel. The secondary mass (also called secondary flywheel) is connected to the clutch. The two masses are attached to each other via a bearing and the secondary mass is thus free to rotate relative to the primary mass. Torque is transferred from the primary mass to the secondary mass via springs. These springs can be either arc springs or several smaller springs arranged in arc segments. The springs are divided into two or more sections that are mechanically separated. A typical DMF and the components therein can be seen in Figure 2.2.

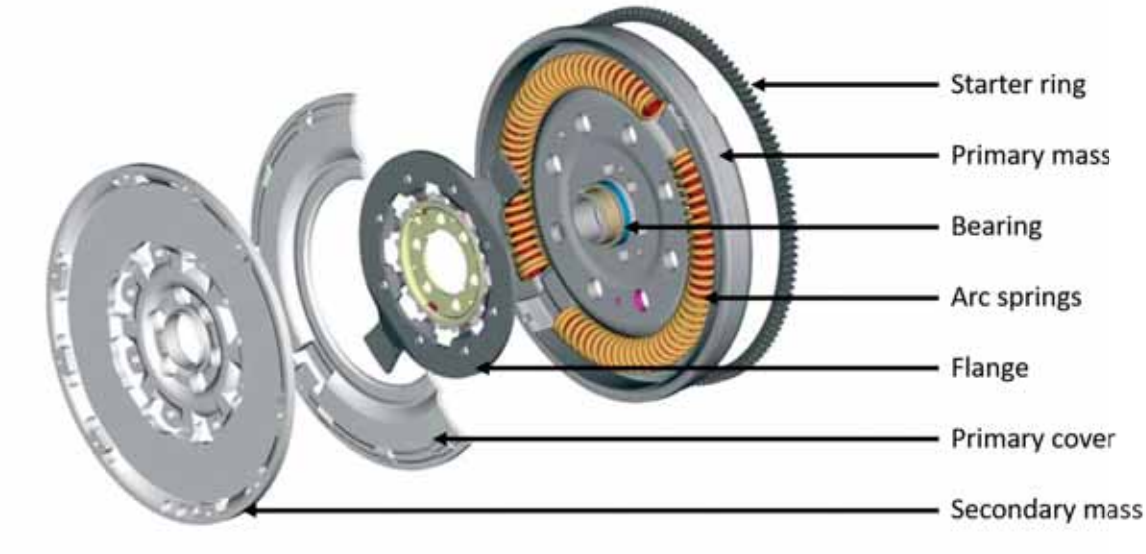

Figure 2.2: *A typical DMF and its components, modified from [4].*

The working principle is that when the primary mass is turned by the engine it will compress the springs which will produce a torque on the flange connected to the secondary mass. The secondary mass will thus turn and if the clutch is engaged and the gearbox is not in neutral gear the vehicle will move.

A DMF reduces the torque and speed irregularities from the engine in primarily two ways. Firstly the inertia in each of the primary and the secondary mass reduces the irregularities in the same way as with a conventional flywheel. The second way is that the torque and speed fluctuations are damped by the springs. When the engine fires the resulting torque peak compresses the springs and the torque is then transferred to the secondary mass. This can give a more even torque to the components downstream of the DMF.

Another advantage of the DMF is that it moves the resonance in the powertrain so that it is not excited at normal operating speeds. In a conventional powertain this resonance lies between 700 and 2000 rpm for passenger cars [5] and between 600 and 1300 rpm for heavy duty trucks. With a DMF this resonance is moved below the idling speed of the engine. This does however mean that the resonance is passed at engine start up which means that damping has to be introduced in the DMF to lower the resonance peaks. The damping will give rise to a hysteresis in the spring torque when the direction of relative rotation is changed.

The negative aspect of the DMF is that apart from being more complex than a conventional flywheel a DMF has some internal friction. As discussed in the previous paragraph this fricton is needed to dampen resonance peaks but during normal driving it decreases the efficiency.

One part of this friction is caused by the springs being pressed towards the outer edge of the channel they slide in [6]. This effect comes from both the centrifugal force and from the compresion of the springs. The compression of the springs will generate both a tangential force and a normal force. The normal force will increase the friction together with the centrifugal force [7].

One way of reducing this friction is to add grease in the spring channel to make the springs slide more easily. The introduction of grease means that the friction in the DMF will depend on the temperature of the grease and thus on the temperature of the DMF. The grease will however introduce viscous friction [8]. This friction is a result of the speed difference between the primary and secondary mass in combination with the viscosity of the grease.

One problem that could potentially occur with DMF:s due to the internal friction is that the springs get stuck and are thus unable to dampen the torsional vibrations. This can cause the isolating effect of the DMF to be eliminated since the springs act like a rigid wall [6]. This means that the rest of the drive train has to absorb the vibrations that the DMF was supposed to dampen. One way of reducing this problem is to introduce sliding shoes as can be seen in Figure 2.3. The sliding shoes are made of polymeric material and positioned between the springs and the spring channel. The sliding shoes change the friction properties since there is no longer metal to metal contact between the springs and the spring channel. This prevents the springs from getting stuck.

Figure 2.3: *Sliding shoes on a DMF arc spring [6].*

AB Volvo have used DMF:s in their FH16 models but they were replaced by conventional flywheels. The DMF that was in production has three spring segments that consist of straight springs arranged in arc segments and connected by sliding shoes. The springs do not have the same stiffness which makes the stiffness curve non linear. The stiffness curve as a function of angle difference between the primary and secondary mass is shown in Figure 2.4. As can be seen the stiffness changes at 2.3 and 13.1 degrees and the maximum angle difference (at maximum allowed torque) is 17.9 degrees. From the stiffness curve the stiffness of the DMF can be approximated as in Table 2.1.

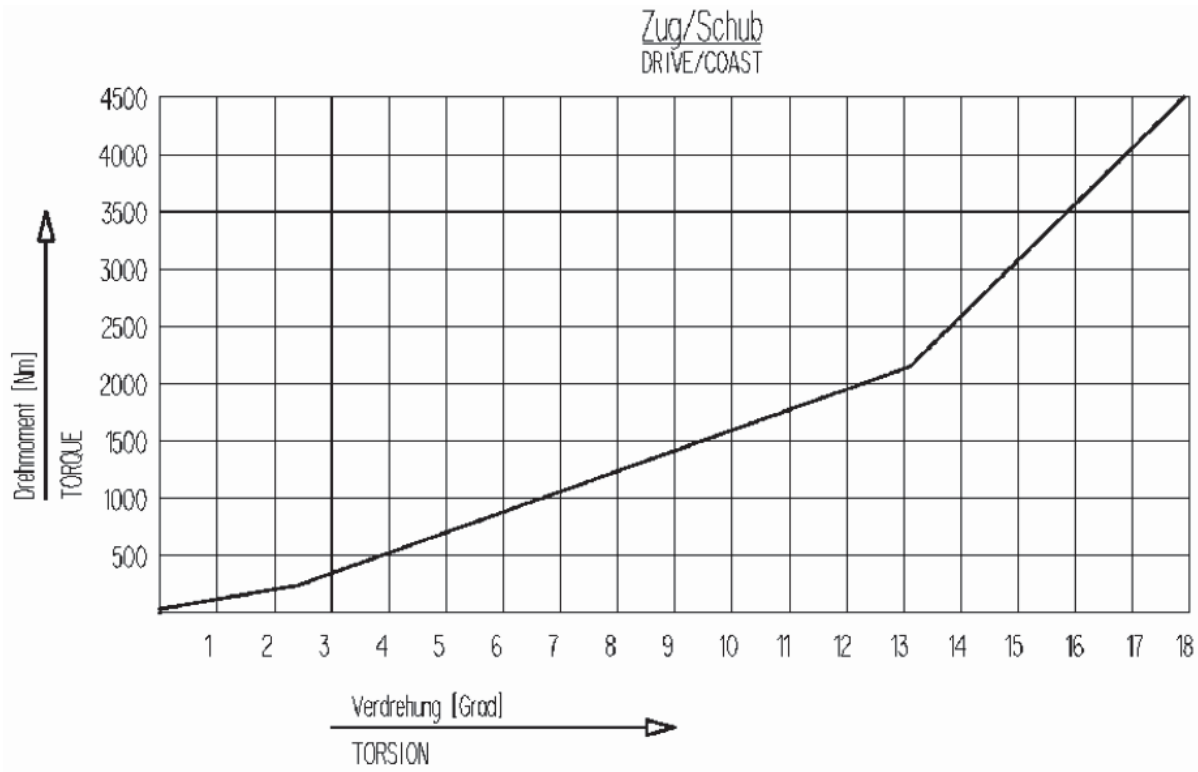

Figure 2.4: *Stiffness curve of the AB Volvo DMF [9].*

Table 2.1: Stiffness of the DMF.

Angle difference [°]	**Stiffness** [Nm/rad]
0.0 - 2.2	7 162
2.2 - 13.1	9 879
13.1 - 17.9	28 051

2.3 Previous work

There has been a lot of research done on DMF:s but most of the literature found has been for passenger cars. The reason for this is that DMF:s are more common in passenger cars than in commercial vehicles. The author has struggled to find research within the scope of this project which is DMF:s for commercial vehicles. Even though there are more differences between a passenger car and a heavy truck than the size of the engine the methodology used for research on DMF:s for passenger cars can be of interest and is presented in this section.

2.3.1 Physical experiments

Mainly two approaches of performing physical experiments on a DMF have been found. The first method is that either the primary or the secondary mass of the DMF is held stationary and an oscillating torque is applied to the other side. This method is presented in [10] and [11] where the secondary mass is stationary and in [7] where the primary mass is fixed. With this method it is possible to analyse the stiffness of the springs by applying either a torque and measuring the angle difference between the two masses or vice versa. Due to that an oscillating torque is applied the hysteresis in the DMF can also be studied.

The second approach is to have some sort of brake connected to the secondary mass. This is done to be able to have an oscillating torque with a mean value greater than zero whilst rotating both the primary and secondary mass. In [10] and [11] this is done via attaching a half shaft to the secondary mass and in the other end of the halfshaft attach a disc brake. The brake is then activated to get the requested torque level. Another way of solving this is presented in [12] and [13] where two electric motors are used, one for each side of the DMF.

The only literature found where DMF:s for commercial vehicles have been used are internal AB Volvo reports. In these reports a full driveline has been used and the property studied has been torsional vibration on the gearbox input shaft rather than the dynamic friction which is the property of main interest in this project. One thing that can be noted from these reports is the method of measuring the rotational speed. In [14] and [15] magnetic pickups are used and in [16] a magnetic pickup is combined with a laser tachometer.

2.3.2 Simulation

Two main approaches of modelling a DMF have been found when studying the literature. The first and simplest approach is to model the DMF as a linear spring damper model as shown in Figure 2.5 and presented in [7], [10], [11], [17] and [18]. Validation of this is done with promising results with test set ups described in section 2.3.1 in [7], [10] and [11]. In [19] a linear model of the DMF is used to predict the instantaneous engine torque and the results are close to experimental values for steady state operation.

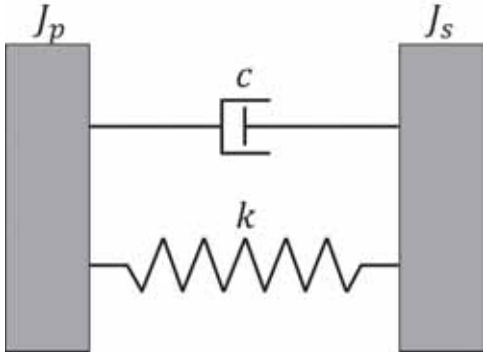

Figure 2.5: *Linear spring damper model.*

The second method is a non linear approach where the arc springs are split into two or more segments and friction is introduced between the spring masses and the spring channel as shown in Figure 2.6. This method is presented in [7], [12], [18] and [20]. The friction in this model is dependent on the force that acts radially on the springs. Since the centrifugal effects are contributing to this force the friction model is speed dependent. The springs are massless in the model but the spring masses is needed to compute the effect of the centrifugal force. This type of non linear model for DMFs is validated using measurement data in [7], [12] and [20].

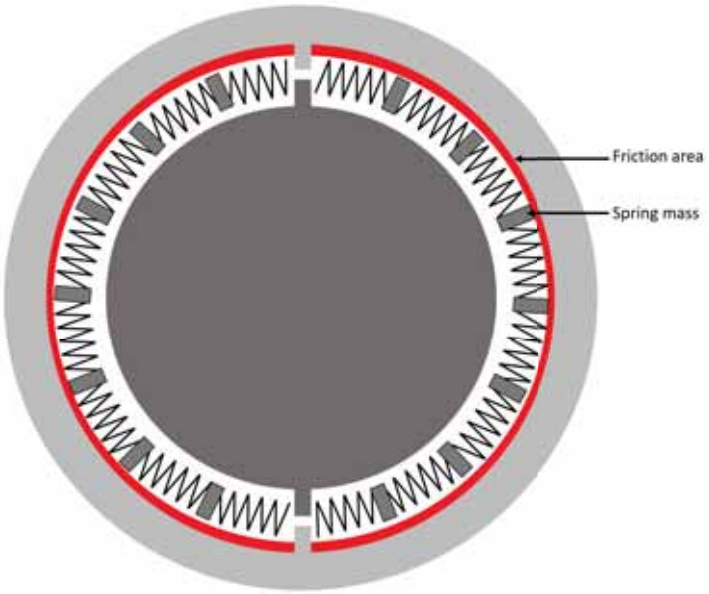

Figure 2.6: *Non linear model with friction and spring masses.*

2.4 Hooke's joint

A Hooke's joint is a type of joint that allows power to be transferred between two rotating shafts with an angle between them. It is often used in propeller shafts in vehicles and in this project it is used to create a nonuniform torque in the physical experiments. The principal design of the joint can be seen in Figure 2.7. Note that the cross that connects the two shafts is rigid and the vectors r_1 and r_2 are thus always orthogonal.

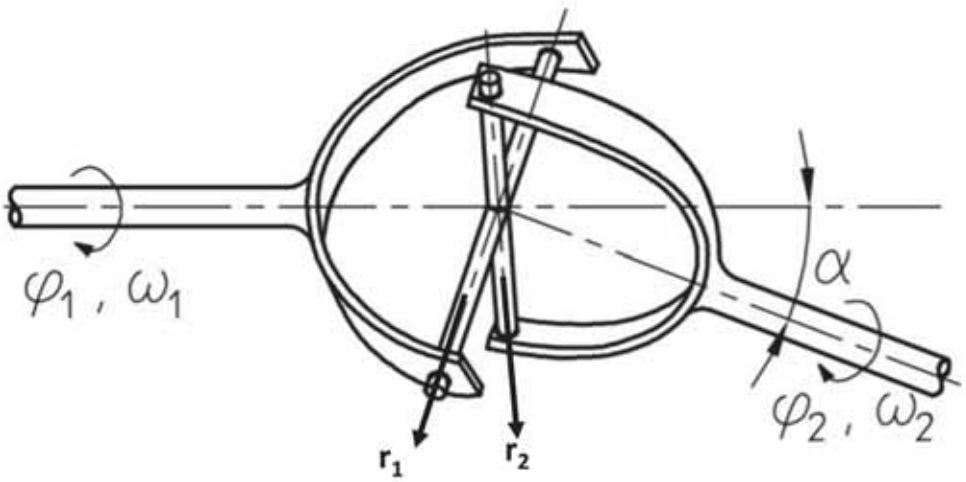

Figure 2.7: *Principal design of the Hooke's joint with the vectors r_1 and r_2 marked, modified from [21].*

The drawback with this kind of joint is that it does not give a constant velocity transfer. This will give a pulsating velocity of the output shaft depending on the angle α. The derivation of the relation between the position, velocity and acceleration of the two shafts is shown in equation (2.1) - (2.10). Figure 2.8 shows the movement of the joint. The two planes represent the planes in which the two vectors r_1 and r_2 move where z is the axis of rotation of part 1 and y is in the intersection of these planes. When the input shaft is rotated an angle φ_1 it causes the vector r_1 to rotate an angle φ_1 around the z-axis in the blue plane. This will cause the vector r_2 to move an angle φ_2 in the red plane.

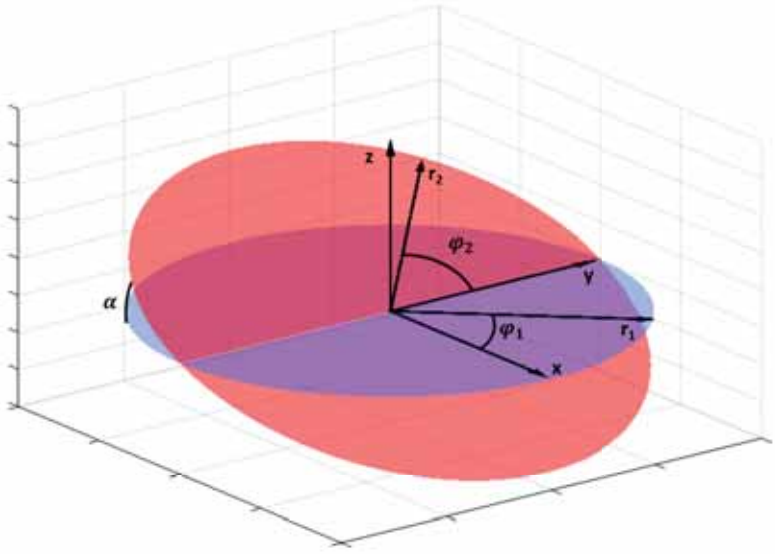

Figure 2.8: *The vectors r_1 and r_2 in a three dimensional coordinate system.*

The vectors r_1 and r_2 can be written in Cartesian coordinates as in equation (2.1) - (2.2).

$$r_1 = [cos(\varphi_1), sin(\varphi_1), 0] \tag{2.1}$$

$$r_2 = [-sin(\varphi_2)cos(\alpha), cos(\varphi_2), sin(\varphi_2)sin(\alpha)] \tag{2.2}$$

Since the cross at the connection point is rigid the two vectors must always be orthogonal to each other. This means that the dot product must be zero. This can be used to derive the relation for the angular position between the two shafts. In equation (2.3) the dot product is calculated which then gives the final expression in equation (2.4).

$$r_1 \cdot r_2 = -cos(\varphi_1)sin(\varphi_2)cos(\alpha) + sin(\varphi_1)cos(\varphi_2) = 0 \tag{2.3}$$

$$tan(\varphi_1) = tan(\varphi_2)cos(\alpha) \tag{2.4}$$

The relation for the velocity is obtained by taking the derivative with respect to time of the expression in equation (2.4). If $\omega_1 = \dot{\varphi_1}$ and $\omega_2 = \dot{\varphi_2}$ is introduced, the resulting expression is as shown in equation (2.5).

$$\frac{\omega_1}{cos^2(\varphi_1)} = \frac{\omega_2 cos(\alpha)}{cos^2(\varphi_2)} \tag{2.5}$$

To eliminate φ_2 the trigonometric formula shown in equation (2.6) can be used with equation (2.4) to obtain the expression for the angular velocity of the output shaft in equation (2.7).

$$cos^2(\beta) = \frac{1}{1 + tan^2(\beta)} \tag{2.6}$$

$$\omega_2 = \omega_1 \frac{cos(\alpha)}{cos^2(\varphi_1)cos^2(\alpha) + sin^2(\varphi_1)} \tag{2.7}$$

This expression can be simplified by using the Pythagorean trigonometric identity. The final expression for the output angular velocity can then be written as in equation (2.8)

$$\omega_2 = \omega_1 \frac{cos(\alpha)}{1 - cos^2(\varphi_1)sin^2(\alpha)} \tag{2.8}$$

The angular acceleration can be obtained by taking the derivative with respect to time for the expression in equation (2.8). By using the trigonometric formula shown in equation (2.9) the final expression for the acceleration in equation (2.10) can be written.

$$2cos(\beta)sin(\beta) = sin(2\beta) \tag{2.9}$$

$$\dot{\omega}_2 = \dot{\omega}_1 \frac{cos(\alpha)}{1 - cos^2(\varphi_1)sin^2(\alpha)} - \omega_1^2 \frac{cos(\alpha)sin^2(\alpha)sin(2\varphi_1)}{(1 - cos^2(\varphi_1)sin^2(\alpha))^2} \tag{2.10}$$

As can be seen the angular acceleration of the output shaft will be dependent on the angular position of the input shaft φ_1, the angular velocity and acceleration of the input shaft and on the joint angle α.

2.5 Mechanics

It is of importance to do calculations of shear stress and bending stiffness of parts used in the experimental set up. This is vital since high levels of shear stress could potentially break or fatigue the parts and high levels of bending in the parts will give large deflection angles that will affect the results. Another important property is the moment of inertia of each part. Together with the angular acceleration this determines the torque needed to rotate the part in question. In this project only parts that can be approximated as tubes with inner diameter d_i and outer diameter d_o are considered and the equations below will thus only concern this geometry.

The shear stress can be calculated using equation (2.11) where the section modulus in torsion W_v can be obtained from equation (2.12) and M_v is the applied torque [22].

$$\tau_v = \frac{M_v}{W_v} \tag{2.11}$$

$$W_v = \frac{\pi \left(d_o^4 - d_i^4\right)}{16 d_o} \tag{2.12}$$

The deflection angle due to an applied torque M_v can be calculated as in equation (2.13) where K is the section factor of torsional stiffness and calculated in equation (2.14), L is the length of the tube and G is the shear modulus [22].

$$\Theta = \frac{M_v L}{GK} \tag{2.13}$$

$$K = \frac{\pi \left(d_o^4 - d_i^4\right)}{32} \tag{2.14}$$

The equation for the moment of inertia for a tube is shown in equation (2.15) where m is the mass of the tube [23].

$$I = \frac{m}{8} \left(d_o^2 - d_i^2\right) \tag{2.15}$$

2.6 Newmark-β method

The Newmark β method is a numerical method of solving differential equations first presented by Nathan M. Newmark in 1952. In this section the method will be derived based on [24] and [25].

Firstly the general equation of motion for a second order system is observed in equation (2.16).

$$\mathbf{M}\ddot{\mathbf{x}} + \mathbf{C}\dot{\mathbf{x}} + \mathbf{K}\mathbf{x} = \mathbf{p}(t) \tag{2.16}$$

If it is assumed that the initial conditions of $\mathbf{x}$ and $\dot{\mathbf{x}}$ are known the initial acceleration can be calculated as in equation (2.17).

$$\ddot{\mathbf{x}}_0 = \mathbf{M}^{-1}\left(\mathbf{p}_0 - \mathbf{C}\dot{\mathbf{x}}_0 - \mathbf{K}\mathbf{x}_0\right) \tag{2.17}$$

In [25] Newmark states that the position $\mathbf{x}$ and the velocity $\dot{\mathbf{x}}$ in the next time step $n+1$ can be expressed as in equation (2.18) - (2.19) where h is the time interval and β and γ are parameters that can be chosen to get different types of solutions.

$$\mathbf{x}_{n+1} = \mathbf{x}_n + h\dot{\mathbf{x}}_n + \left(\frac{1}{2} - \beta\right)h^2\ddot{\mathbf{x}}_n + \beta h^2\ddot{\mathbf{x}}_{n+1} \tag{2.18}$$

$$\dot{\mathbf{x}}_{n+1} = \dot{\mathbf{x}}_n + (1-\gamma)\,h\ddot{\mathbf{x}}_n + \gamma h\ddot{\mathbf{x}}_{n+1} \tag{2.19}$$

By combining equation (2.16), (2.18) and (2.19) the expression for the acceleration $\ddot{\mathbf{x}}_{n+1}$ in equation (2.20) can be obtained.

$$\ddot{\mathbf{x}}_{n+1} = \left[\mathbf{M} + \mathbf{C}\gamma h + \mathbf{K}\beta h^2\right]^{-1}\left(\mathbf{p}_{n+1} - \ddot{\mathbf{x}}_n\left((1-\gamma)\,h\mathbf{C} + \left(\frac{1}{2} - \beta\right)h^2\mathbf{K}\right) - \dot{\mathbf{x}}_n\left(\mathbf{C} + h\mathbf{K}\right) - \mathbf{x}_n\mathbf{K}\right) \tag{2.20}$$

Newmark proposes a value of $\gamma = \frac{1}{2}$ [25]. If this value of γ is used and the value of β is chosen to be $\beta = \frac{1}{4}$ the constant acceleration method is obtained which is unconditionally stable [24].

2.7 Measurement technique

2.7.1 Measuring torsional vibrations

Measuring of torsional vibrations can be done in several different ways. The techniques used in this project is magnetic pickups and optical sensors with zebra tape. These two techniques along with a criterion for minimum number of pulses per revolution will be presented here.

Magnetic pickups

A magnetic pick up works by sensing the change in the magnetic field. The change in magnetic field is used to generate an output signal according to Faraday's law. This can be seen in equation (2.21) where U is the voltage of the output signal, N is the number of windings in the sensor coil and Φ is the magnetic flux [26].

$$U = -N\frac{d\Phi}{dt} \tag{2.21}$$

This can be utilized for a flywheel by using the sensor to measure the change in the magnetic field caused by the gear teeth of the starter ring. The accuracy of the signal will depend on how many pulses per revolution (PPR) there are in the signal . In the case of measuring the rotational speed of the flywheel this translates to the number of gear teeth on the starting ring. One advantage of this type of sensor is that since the output is generated by the change in the magnetic field it does not need any power supply. This does however cause some negative effects as well since the shape and amplitude of the output signal will vary with the rotational speed of the measured object. This may lead to accuracy problems at low speeds [26].

Optical sensors with zebra tape

An optical sensor works by emitting light and registering change in the reflected light. It can be used on a surface where the contrast is alternating and thus the reflected light is alternating. One way of achieving this is by using a zebra tape. Zebra tape is a tape that has alternating black and white fields and can be fastened to a surface to generate a controlled change in the reflected light. In Figure 2.9 zebra tape has been fastened to a DMF. One potential problem is if the ends of the zebra tape do not match. This will create an error since one field do not have the same size as the other fields. One way of solving this is by creating one large overlapping field at the mating point and using a correction algorithm [26]. An example of how to create an overlapping mating point can be seen in Figure 2.10.

Figure 2.9: *Zebra tape fastened on a DMF.*

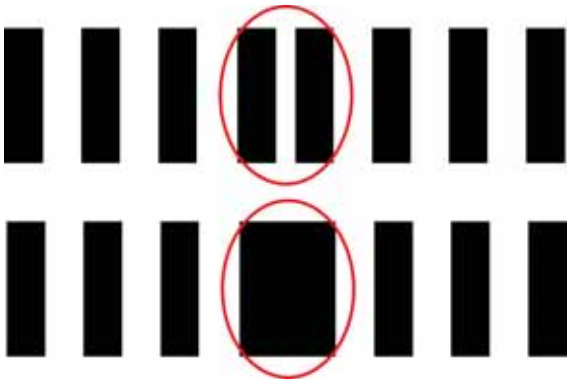

Figure 2.10: *Example of overlapping mating point.*

Number of pulses per revolution

To be able to correctly analyse the data collected from measurements of rotational speed it is important to have high enough resolution. This translates to how many PPR the measured signal has. The required resolution is dependent on which order that is studied. One way of selecting the minimum number of PPR is presented in [26]. The method is based on the Nyquist-Shannon sampling theorem. If the Nyquist-Shannon sampling theorem is studied in the angle domain the condition in equation (2.22) can be set where O_{max} is the maximum order that is to be studied.

$$PPR_{min} = 2O_{max} \tag{2.22}$$

2.7.2 Torque measurement

When measuring torque there are a lot of measurement uncertainties to consider. In equation (2.23) - (2.32) the equations to calculate the total uncertainty based on [27] is presented where U is the total uncertainty. The needed sensor properties are obtained from the data sheet of the sensor, from calibration or from the measured test data. A list of all the properties and where to find them can be found in Appendix A.

$$U = \sqrt{U_{TK0}^2 + U_{TKC}^2 + U_{lh}^2 + U_{b'}^2 + U_b^2 + U_K^2 + U_r^2 + U_p^2 + U_s^2 + U_a^2} \tag{2.23}$$

$$U_{TK0} = M_{nom} TK_0 \frac{\Delta T}{10K} \tag{2.24}$$

$$U_{TKC} = M_{ap} TK_C \frac{\Delta T}{10K} \tag{2.25}$$

$$U_{lh} = M_{nom} d_{lh} \tag{2.26}$$

$$U_{b'} = k \frac{M_{ap}}{\Delta M_{ref}} \Delta M_{ref} \sigma_{rel} \tag{2.27}$$

$$U_s = \left(\frac{n_{ap}}{n_{nom}} \right)^2 d_{speed} M_{nom} \tag{2.28}$$

$$U_b = \frac{k}{2} max[b(M)] \tag{2.29}$$

$$U_K = M_{nom} d_c \tag{2.30}$$

$$U_p = M_{nom} d_{para} \frac{L_{para}}{L_{para,ref}} \tag{2.31}$$

$$U_r = \frac{M_{ap,max} - M_{ap,min}}{2M_E} f_r(M) \tag{2.32}$$

3 Method

3.1 Strategy

The object of both the measurements and the simulations was to analyse the friction properties of the DMF. The approach chosen was to perform measurements with a number of controlled inputs to the system and try to measure the friction losses. The test set up used was then simulated with a linear spring damper model. The damping coefficient in the simulation model was adjusted to fit the measured results.

3.2 Measurements

3.2.1 Test set up

Basic test set up

The test rig used is driven by an electric motor that drives a large flywheel with an inertia of 40 kgm^2 via a belt transmission. The large flywheel and electric motor can be turned around a point below the Hooke's joint in the propeller shaft. By doing this a nonuniformity in the speed and acceleration after the Hooke's joint can be created. The test object, in this case the DMF, is fastened to a shaft in a sleigh that has the same hole pattern as a crank shaft. The sleigh is a console where the test object is fastened, the sleigh itself is then mounted in the test rig.

A picture of the test set up can be seen in Figure 3.1. The DMF and clutch are not visible since they are located inside the flywheel and clutch housing. Two set ups were used in this test rig, one with the clutch mounted to the secondary mass and one without the clutch. This is done to get two levels of inertia at the secondary mass. The secondary mass of the DMF and the clutch can rotate freely.

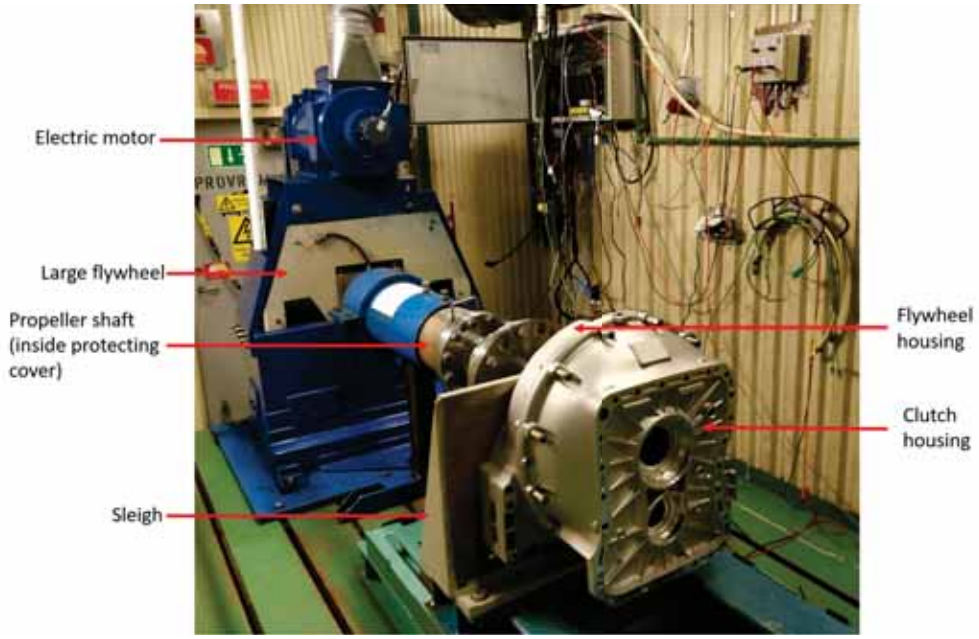

Figure 3.1: *The test set up with the large flywheel and electric motor in the background and the DMF inside the flywheel and clutch housing in the foreground.*

Four adapters were used to mount the torque sensor to the propeller shaft and the DMF. In Figure 3.2 the adapters are numbered from 1-4. Adapter 1 already existed at AB Volvo and was used to utilize the cross serration of the propeller shaft. To be able to attach the torque sensor to this side adapter 2 had to be designed and manufactured. On the DMF side of the torque sensor there are two adapters to attach the sensor to the sleigh and ultimately to the DMF. Adapter 3 was designed and manufactured during the project while adapter 4 already existed and similar to adapter 1 it utilizes the cross serration of the sleigh. Note that the torque sensor is placed after the Hooke's joint to be able to measure the nonuniformity in the applied torque. A complete list of the parts used along with some important properties can be seen in Appendix B.

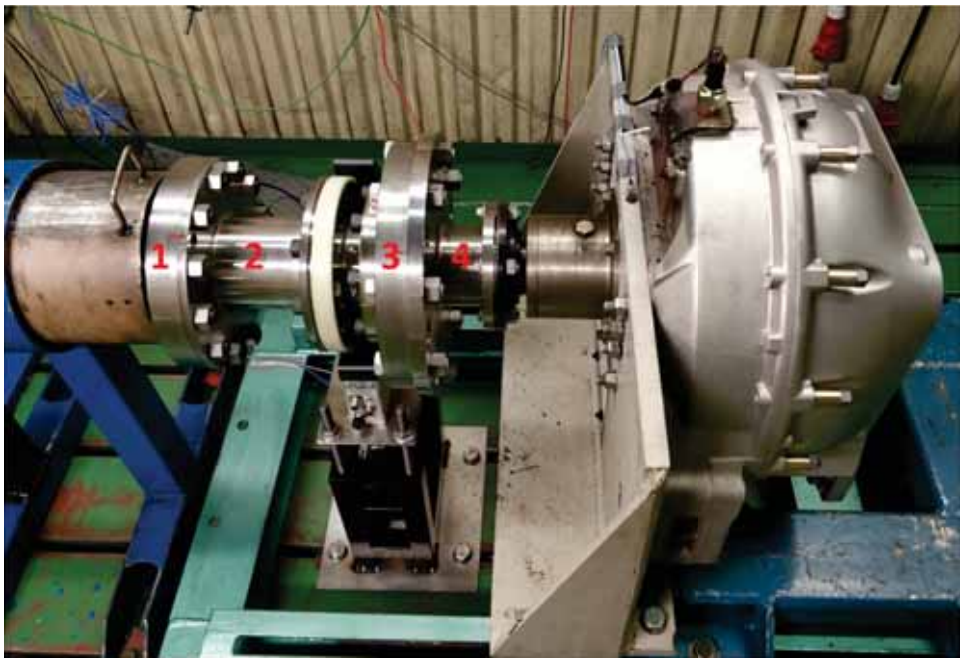

Figure 3.2: *The test set up from the end of the propeller shaft to the clutch housing with the adapters numbered. 1=Adapter 1, 2=Adapter 2, 3=Adapter 3, 4=Adapter 4.*

Temperature dependency

As mentioned in section 2.2 the temperature of the grease inside the DMF is of importance for the friction. A higher temperature in the grease will mean that it has a lower viscosity which means different friction properties. When the DMF is rotated the energy generated from this will heat up the grease. This means that if the temperature is not controlled the grease will have a higher temperature at high speeds since the generated energy is increasing with speed. Since the final output of the tests is to try to estimate the friction inside the DMF it is therefore of importance to control the temperature of the grease.

To handle this, a hole was made in the flywheel housing and a heat gun was attached to a overhead crane to blow hot air on to the DMF. The temperature of the surface of the DMF was measured with an infra red sensor. The surface chosen was the surface where the crank shaft is normally attached since this gave the smallest distance between the springs and measured surface. The DMF was heated up until the surface temperature was approximately 80° C and was then kept at this temperature during the tests. This temperature was chosen since it is the temperature inside the the flywheel and clutch housing at normal driving.

Measurement points

The measurement points of the speed of the primary and secondary mass can be seen in Figure 3.3 where they are marked "PM" and "SM" respectively. The speed of the primary mass is measured with a magnetic pick up sensor at the starter ring. This means that the accuracy will be dependent on the number of teeth of the starter ring which is 153. Speed measurement of the secondary mass is done with an optical laser tachometer and attaching zebra tape on the secondary mass. The optical laser tachometer is screwed in to a hole made in the flywheel housing. The accuracy of this measurement will depend on the number of black and white fields on the used zebra tape which is 60 and is equal to 60 ppr. If the accuracy of the measurement of the primary and secondary mass is compared to the theory presented in Section 2.7.1 it can be concluded that the accuracy is well above what is needed to measure the main order of concern which is the second order. The speed of the rig flywheel was measured with a magnetic pick up at the back of the rig and the accuracy was the same as for the secondary flywheel, 60 ppr.

To measure the torque a HBM T12 10 kNm was used. It was placed between the propeller shaft and the DMF to be able to measure the nonuniformity in the torque. In Figure 3.3 the torque sensor is marked "TS". The frequency output port from the sensor was used to ensure maximum possible accuracy. The measured torque was the torque needed to rotate all parts downstream of the sensor. This includes two adapters, input shaft to the sleigh, the primary mass and the secondary mass.

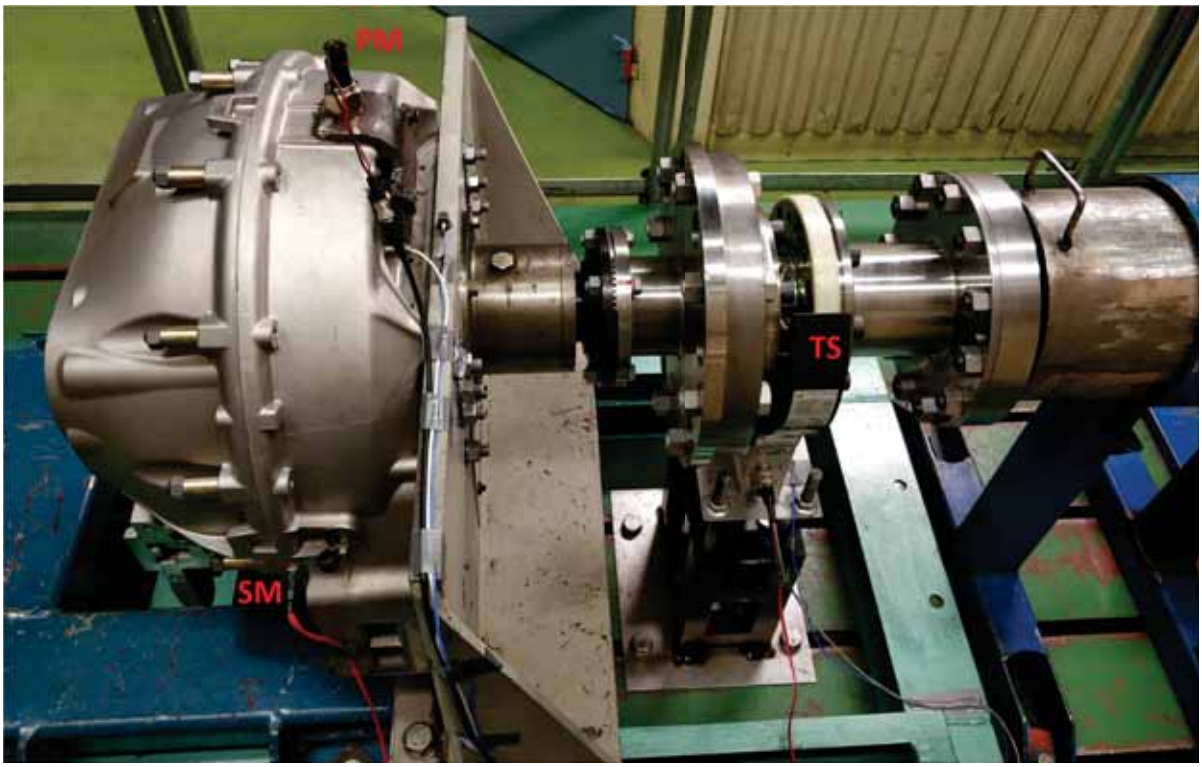

Figure 3.3: *The measurement points of the speed of the primary (PM) and secondary (SM) mass and the placement of the torque sensor (TS).*

The temperature of the DMF was measured in two ways. As mentioned an infra red sensor was used to measure the surface temperature of the side closest to the engine. The mounting of this sensor can be seen in Figure 3.4 where the sensor is marked "IR". A stable surface temperature does however not necessarily mean that the temperature inside the DMF and in the grease is stable. To measure the temperature of the grease would be difficult since this would mean that modifications to the DMF would have to be made that could potentially damage the friction surface or even worse allow the grease to leak out from the closed part of the DMF where it should be located.

The solution to the problem of measuring the temperature of the grease was to measure the temperature inside the material close to the grease. An assumption was then made that if this temperature is stable, the heat of the grease is stable as well. The sliding surface of the springs is located at a radial distance 205 mm from the center of the DMF and 20 mm from the surface facing the engine. As can be seen in Figure 3.5 holes were drilled in to the DMF and thermocouples type K were inserted in these holes. The temperature from the four thermocouples were then logged with an MSR145 logging device. The holes were drilled at a radial distance of 208 mm from the center of the DMF and they were made 22 mm deep into the surface facing the engine.

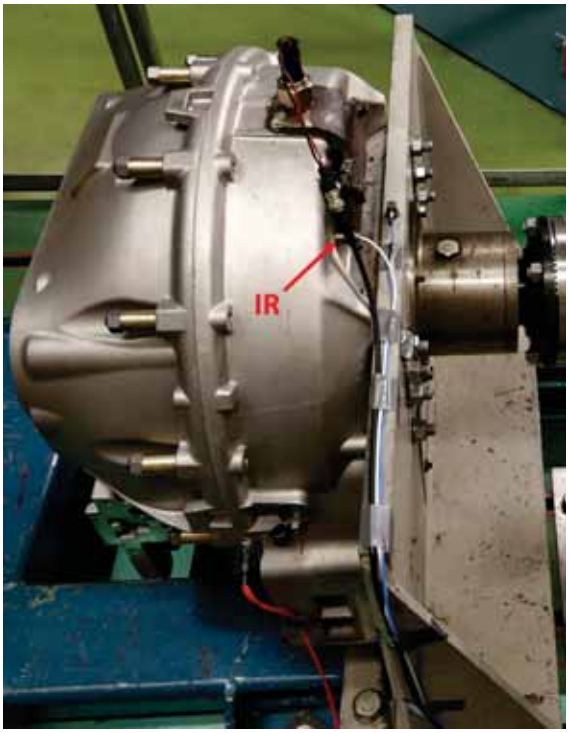

Figure 3.4: *Placement of the infra red sensor (IR).*

Figure 3.5: *Measurement points of the temperature inside the DMF.*

Two triaxial accelerometers was used to be able to detect possible sources of errors if the tests did not go as planned. They were placed at the sleigh base and on the surface where the stationary part of the torque sensor was fastened. The final two measurements were the ambient temperature and the temperature of the air inside the flywheel housing. These temperatures were both measured with thermocouple type K. A complete wiring scheme along with part name and number of sensors and measuring equipment used can be seen in Appendix B.

Adapters

In order to be able to use the torque sensor in the test rig some adapters were used to attach it in the correct way which can be seen in Figure 3.2. The adapters used were both already existing ones and adapters designed and manufactured during the project. The final drawings of the designed and manufactured adapters can be seen in Appendix B.

The adapters were designed with the aim that they should be usable for AB Volvo in future projects as well as in this project. Because of this, fatigue of the adapters had to be considered and the shear stress was set to a limit of 100 MPa at a load of 40 kNm. It was also taken into account that the adapters should be stiff enough so they would not deform significantly during the experiments and thus affect the results. Another aim when designing the adapters was to make them as light as possible, both to make them easier to handle but also to keep the moment of inertia as low as possible. The process of the calculations done in the design process is explained in the following paragraphs. When performing the calculations for the adapters it was assumed that they could be approximated as a number of tubes with different inner and outer diameter joined together.

The shear stress is calculated as in equation (2.11). By combining this equation with equation (2.12) an expression for the inner diameter can be written as in equation (3.1). This equation was used to make sure that the shear stress did not exceed the set limit whilst as large hole as possible could be made in the center of the adapters to make it as light as possible.

$$d_i = \sqrt[4]{d_o \left(d_o^3 - \frac{16 M_v}{\pi \tau_v} \right)} \tag{3.1}$$

The total rotational stiffness K_Θ of the adapters can be expressed as in equation (3.2) where Θ_i is the deflection angle for each part of the adapters calculated as in equation (2.13) and M_v is the applied torque. A high rotational stiffness is desirable for the adapters since this means that the deflection angles will be small and thus not effect the results from the physical experiments significantly.

$$K_\Theta = \frac{\sum \Theta_i}{M_v} \tag{3.2}$$

The last property of the adapters to calculate is the moment of inertia. For the adapters designed during the project the virtual model in Creo Parametric was used to calculate this. To approximate the moment of inertia for the already existing adapters equation (3.3) was used where I_i is the moment of inertia for each part of the adapter calculated as in equation (2.15).

$$I = \sum I_i \tag{3.3}$$

Modification of clutch disc

The principle design of a clutch disc is explained in Figure 3.6. The function of the damper springs is to dampen torsional vibrations by allowing relative motion between the driven disc and the hub. The pre damper takes care of the engine speed irregularities when idling in neutral gear.

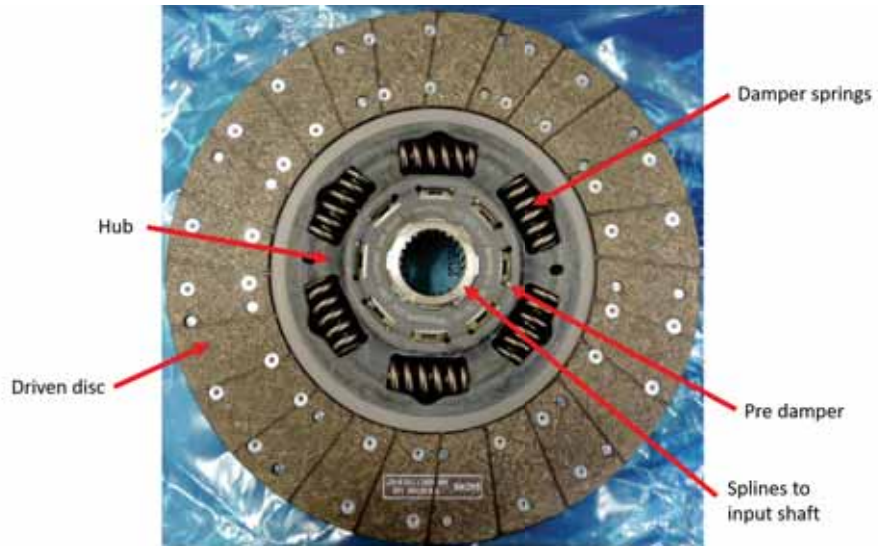

Figure 3.6: *Principle design of a clutch disc.*

In the physical experiments in this project the aim is to measure relative motion of the DMF. To get as accurate result as possible all other parts should thus rotate as little as possible relative to the DMF. This means that the ideal case would be to have a driven disc that is connected rigidly to the hub. Therefore a standard clutch disc was modified accordingly.

The tests are performed with high levels of angular acceleration. It is therefore of high importance to know the moment of inertia as precise as possible for each part. This means that as small modifications as possible should be made to the clutch disc. In the test set up no input shaft is used and the secondary side of the DMF (along with the clutch) is rotating freely. This means that the only torque available to turn the hub relative to the driven disc is the inertial moment of the hub. The inertia of the hub was estimated to be so small that the damper springs would never be compressed more than the preload they have in assembled state. One potential problem could however be the pre damper. This was solved by welding the pre damper and the hub together as shown in Figure 3.7.

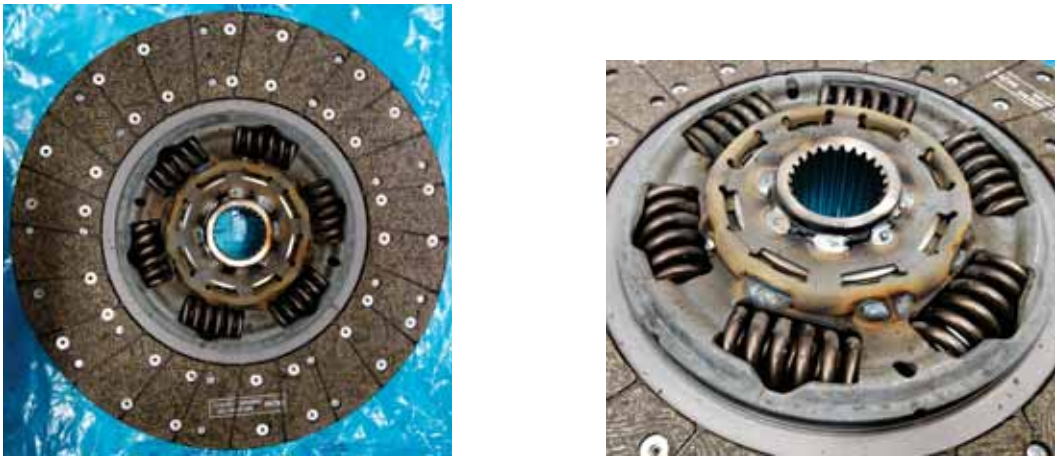

Figure 3.7: *Clutch disc with the pre damper welded to the hub.*

3.2.2 Operating points

Two parameters can be varied in the rig to get different levels of angular acceleration, which means different levels of torque, and different levels of rotational speed. Those parameters are the rotational speed of the electric motor driving the rig and the angle of the Hooke's joint in the propeller shaft. A third way of varying the torque level was added by having two set ups of the flywheel. One without and one with a mounted clutch. When the clutch is mounted the moment of inertia of the secondary mass will increase which means that the torque needed to accelerate the secondary mass will be different.

The tests were performed as follows. The desired angle of the Hooke's joint was set by rotating the electrical motor and rig flywheel. After this the DMF was heated up during rotation to around 80° C in surface temperature. The range of rotational speeds was then covered in steps of 100 rpm. The rig was accelerated up to the desired speed and then kept steady at this speed for about 60 s and then decelerated to standstill. This was done until the whole speed range was covered or until the amplitude of the measured torque became more than 4500 Nm. When this was done a speed of 700 rpm was tested again to be able to verify that the results did not drift during the measurements. The surface temperature of the DMF was kept at around 80° C for all measurements. The speed range covered for all angles tested can be seen in Table 3.1.

Table 3.1: Speed interval for all angles of the Hooke's joint.

Angle	**Rotational Speed Range**
1°	200-1500 rpm
3°	200-1500 rpm
5°	200-1500 rpm
7°	200-1300 rpm
10°	200-1200 rpm
12°	200-1200 rpm
14°	200-1100 rpm
15°	200-1100 rpm

The same operating points were used for both the case with and without the clutch with one difference. When performing the tests without the clutch mounted it was discovered that the two smallest angles of the Hooke's joint were too small to give any valuable results. Therefore these angles were not used with the clutch attached.

3.2.3 Post processing

When all measurement data had been gathered it was post processed in a way that will be described in this section. The used software was DEWEWSoft X2, imc FAMOS and MATLAB.

Correction of speed signal

As mentioned in section 2.7.1 one problem with using zebra tape to measure angular speed is the mating point of the zebra tape. Since one of the fields will be either larger or smaller than the other mating field due to the small overlap it will give rise to a momentary false peak in angular speed and this has to be corrected afterwards. The diameter of the DMF was so large that it was not enough to use one zebra tape. Thus, there were two mating points. There can also be false peaks in angular speeds due to other measurement errors that also have to be corrected, this can for example be if there is dirt on one of the white fields of the zebra tape. There are software that can be used to correct this but no such software was available so a script that did this correction was written.

The points where there is a peak in angular speed will give a large acceleration peak which can be utilised to correct the signal. The way this was done in this project was that the angular acceleration was computed and analysed. If the angular acceleration was larger than $\frac{1}{6}$ of the maximum acceleration an interpolation in speed was made between the point before and after the acceleration peak. An example of measurement before and after this correction can be seen in Figure 3.8. Note that the correction points which corresponds to the mating point of the zebra tape are placed at 240 and 360°. This is done to avoid a false second order in the measured signal which would be the case if they were placed symmetrically. In the figure it can also be noted that the measured signal is not smooth even where there are no mating points. This is due to both noise and that the resolution of the printer gives rise to small differences in how large the black fields are. This error can be dealt with by filtering the signal.

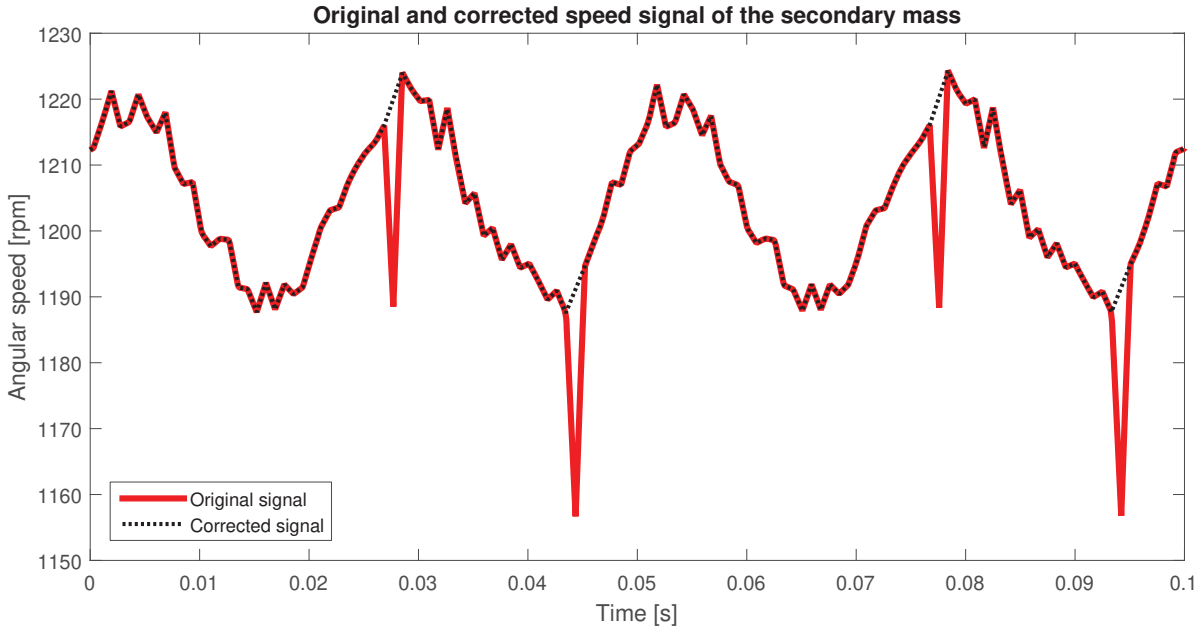

Figure 3.8: *Original and corrected speed signal of the secondary mass.*

Filtering

To get rid of the measurement noise in the measured signals they need to be filtered before they are analysed. This was done by using a low pass order tracking filter. This type of filter filters out the frequency content of the signals that are of higher order than desired. The specific filter used in this project is a filter in imc FAMOS called "OtrTrackingLowPassZ". This filter does not phase shift the filtered signal.

The filtered signals are the angular speed of the primary and secondary mass and the measured torque. To be able to know at what order to set the limit the frequency content of the signals has to be analysed. This was done by analysing the acceleration lapse of the measurement data. For each angle of the Hooke's joint the acceleration lapse up to the highest angular speed was studied. Campbell plots like the one shown in Figure 3.9 were analysed to understand where to set the cut-off order in the low pass filter without filtering too much. In the plot shown the frequency content of the secondary mass with a propeller shaft angle of 7° is shown. A good limit was found to be the eighth order and this was used for all measured data sets.

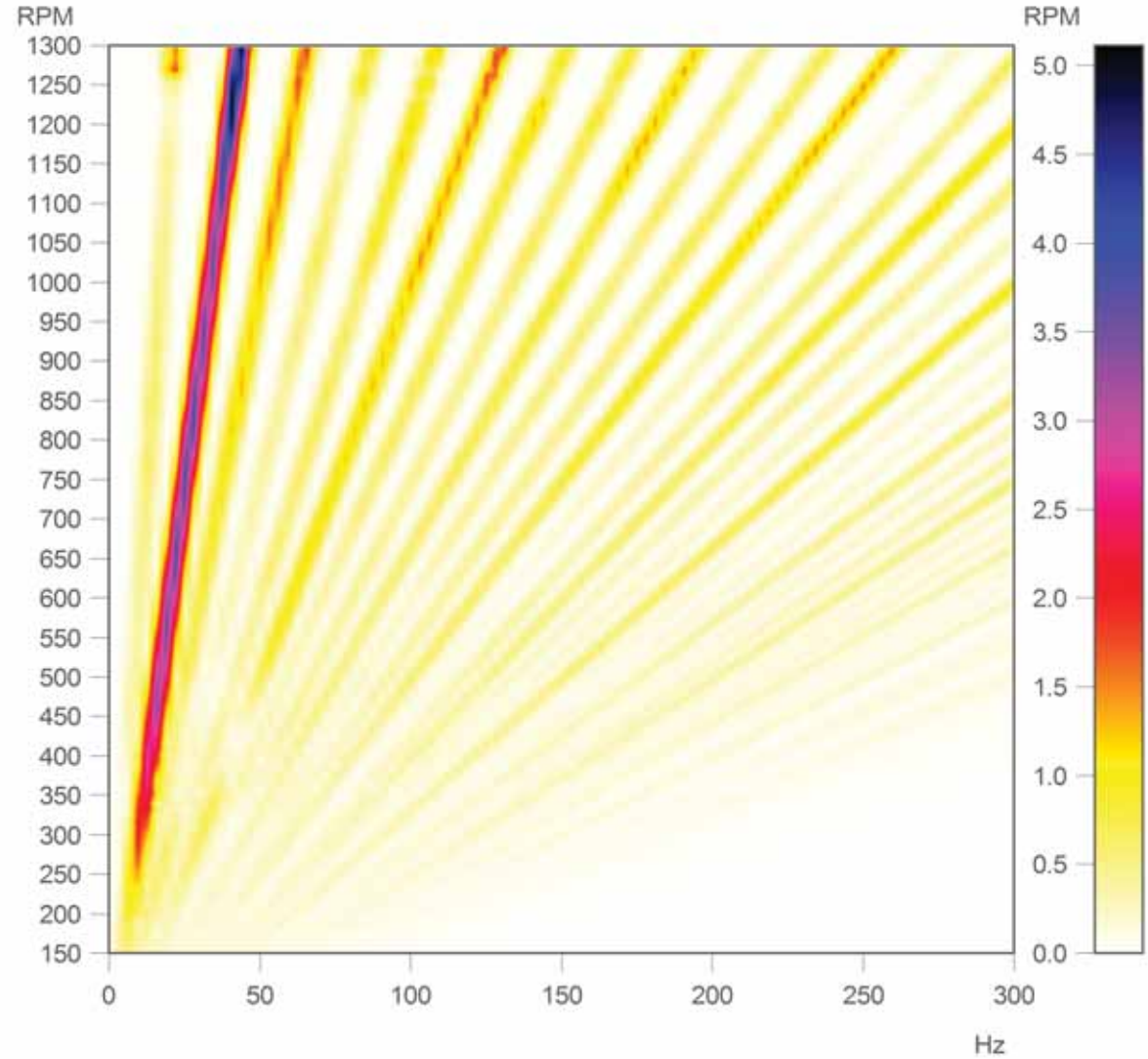

Figure 3.9: *Campbell plot of the speed of the secondary mass with propeller shaft angle of 7°.*

Torque measurement uncertainty

As described in section 2.7.2 there are many factors to consider when calculating the uncertainty of torque measurements. Some of the properties needed to perform these calculations can be found in the data sheet for the sensor while other properties have to be calculated during calibration or be based on experience. The calibration process performed at AB Volvo is a more simple process than the one needed to calculate these properties and they are therefore omitted. The factor based on experience is concerning rotational speed during the measurement. This factor is omitted due to the combination of the author's lack of experience and the fact that the rotational speed during the measurements was well below the nominal speed of the sensor. These simplifications reduce equation (2.23) to the expression seen in equation (3.4).

$$U = \sqrt{U_{TK0}^2 + U_{TKC}^2 + U_{lh}^2 + U_{b'}^2 + U_p^2} \tag{3.4}$$

From this point in the report the measurement uncertainty will be treated as an interval and no detailed calculations will be presented. The interested reader is referred to Appendix A for numerical values of parameters, calculations and estimation of parasitic loads.

3.2.4 Analysis of measured data

The main object of the analysis was to study the friction losses of the system. To do this several results were calculated from the measured data. Since the temperature of the grease in the DMF will affect the friction properties it is of high importance to verify that the measured temperature has been approximately the same for all measurements. When studying the measured temperature inside the DMF it was found that it had been around 55° C for all measurements and that the maximum and minimum temperature had been 62° C and 52° respectively. All measurements were thus considered usable in terms of temperature. The measurements were then analysed to see if the quality of the signals was good enough to perform the required analysis. Four measurement files did not meet the required quality and was thus excluded from further analysis. These files are listen in Table 3.2.

Table 3.2: The excluded operating conditions.

Speed	**Angle**	**Clutch**
400 rpm	14°	No clutch
400 rpm	12°	With clutch
400 rpm	14°	With clutch
400 rpm	15°	With clutch

The first property calculated was the losses in the system. It was assumed that all losses originated from the damping of the DMF. The system is rotating freely, thus, the energy input to the system during one revolution should be zero if the system is loss free. The friction losses could thus be calculated by integrating the power input to the system with respect to time as in equation (3.5). The power input to the system was calculated as the torque measured by the torque sensor T_{inp} multiplied with the difference between the rotational speed of the primary mass ω_p and its mean speed in order to get just the oscillating part of the speed signal. In these calculations it is assumed that the adapters between the torque measurement and the primary mass where the speed of the primary mass is measured are infinitely stiff and thus that a torque measurement in time correspond to the same time stamp of the speed of the primary mass. The loss was calculated for 10, 20, 30, 40 and 50 revolutions and the average was then calculated to get the loss for one revolution.

$$W_{loss} = \int_{t_0}^{t_1} T_{inp}(t) \left(\omega_p(t) - \bar{\omega}_p\right) dt \tag{3.5}$$

The viscous friction of the DMF is dependent on the damping coefficient and the speed difference between the primary and secondary mass. Therefore the speed difference between the two masses had to be calculated. This was done as in equation (3.6) where ω_p and ω_s is the speed of the primary and secondary mass respectively.

$$\omega_{diff} = \omega_p - \omega_s. \tag{3.6}$$

3.3 Simulation

3.3.1 System model

The system used in the measurements can be represented by a linear spring damper model as shown in Figure 3.10. Note that the secondary mass is rotating freely. In the model the primary mass will represent all masses and inertias between the torque sensor and the springs in the DMF. The mass and inertia of the secondary mass and the clutch will be represented by the secondary mass in the model.

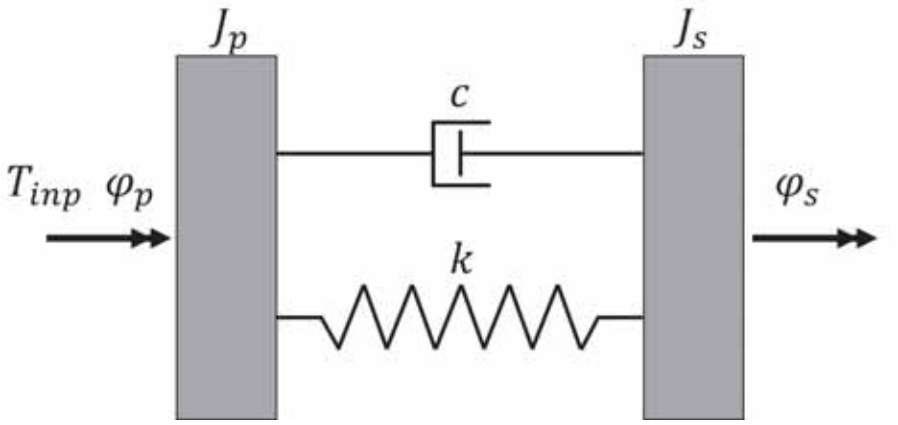

Figure 3.10: *Spring damper model of the test set up.*

3.3.2 Mathematical model

The base for the mathematical model is the model shown in Figure 3.10. If Newtons second law is applied to the system, the equations of motion can be written as in equation (3.7) - (3.8).

$$T_{inp} = J_p\ddot{\varphi}_p + k\left(\varphi_p - \varphi_s\right) + c\left(\dot{\varphi}_p - \dot{\varphi}_s\right) \tag{3.7}$$

$$0 = J_s\ddot{\varphi}_s - k\left(\varphi_p - \varphi_s\right) - c\left(\dot{\varphi}_p - \dot{\varphi}_s\right) \tag{3.8}$$

These two equations form a system of linear differential equations. The system was solved with the Newmark β method. To solve the system with this method the system had to be written on the form shown in equation (2.16). This is done in equation (3.9).

$$\begin{bmatrix} J_p & 0 \\ 0 & J_s \end{bmatrix}\begin{bmatrix} \ddot{\varphi}_p \\ \ddot{\varphi}_s \end{bmatrix} + \begin{bmatrix} c & 0 \\ 0 & c \end{bmatrix}\begin{bmatrix} \dot{\varphi}_p \\ \dot{\varphi}_s \end{bmatrix} + \begin{bmatrix} k & 0 \\ 0 & k \end{bmatrix}\begin{bmatrix} \varphi_p \\ \varphi_s \end{bmatrix} = \begin{bmatrix} T_{inp} \\ 0 \end{bmatrix} \tag{3.9}$$

3.3.3 Simulations before physical experiments

The set up used in the measurements was simulated before the physical experiments were performed. This was done to get an understanding of how the system would behave for a given input. Since the torque input to the system was unknown it was assumed that the primary mass transfers the input angle, speed and acceleration directly to the spring and damper. This reduces the system to look like in Figure 3.11 and the equation of motion as in equation (3.8).

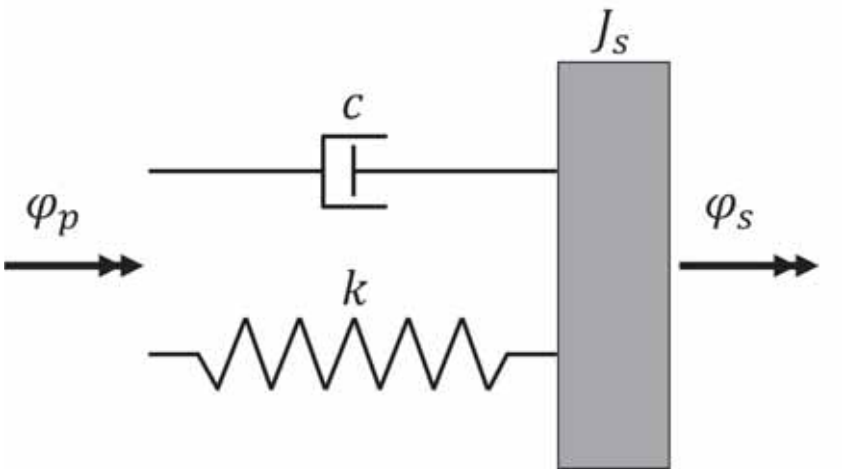

Figure 3.11: *Spring damper model used in the simulations before the physical experiments.*

The angle and speed of the primary mass can be calculated using equation (2.4) and (2.8). The inputs to the system are thus the rotational speed before the Hooke's joint and the angle of the joint. This translates to the speed of the electric motor in the test rig and the angle of the Hooke's joint in the propeller shaft. The system was simulated for all test cases and the angle difference between the primary and the secondary mass was calculated.

Since the damping coefficient of the DMF was unknown an assumption had to be made for the value thereof. In [18] a damping coefficient of c = 5 Nm/(rad/s) is used and this value was used in these simulations as well. To study the effect of a higher damping coefficient simulations with a damping coefficient of c = 10 Nm/(rad/s) were carried out as well. After the first simulations had been performed it was noticed that the angle difference rarely was above 13.1 degrees. Since the stiffness of the DMF changes at this point it was decided to use the lower stiffness which is k = 9879 Nm/rad. The system was simulated with two different inertias. The lower inertia represents the case without a clutch attached and the higher inertia represents the case where the clutch is included in the set up.

The result of the simulations can be seen in Figure 3.12 and 3.13 where the amplitude of the speed oscillation of the secondary mass is plotted for different angles of the Hooke's joint and for both the case with and without the clutch mounted. The influence of a higher damping coefficient can be seen if the two figures are compared. In the simulations with a higher damping coefficient the amplitude is about half of the amplitude simulated with the lower damping coefficient. It can also be seen that larger angles of the Hooke's joint gives larger amplitudes. This is because a larger angle will give higher acceleration levels and thus a larger speed variation. Lastly it can be noted that there seems to be a resonance present in the system. For the higher inertia this seems to be at around 320 rpm and for the lower inertia at approximately 500 rpm.

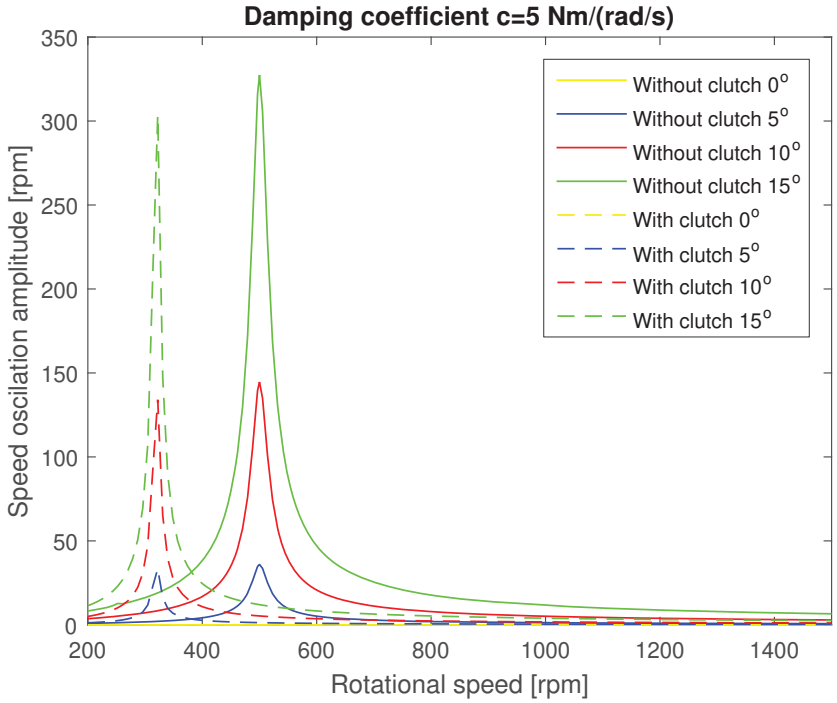

Figure 3.12: *Amplitude of the speed oscillations for the secondary mass with a damping coefficient of 5 Nm/(rad/s).*

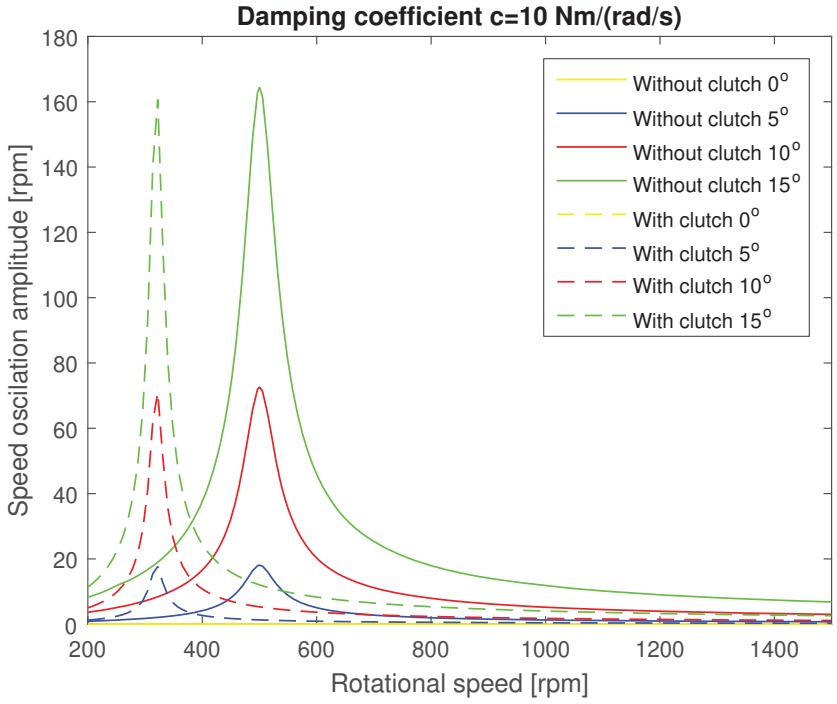

Figure 3.13: *Amplitude of the speed oscillations for the secondary mass with a damping coefficient of 10 Nm/(rad/s).*

3.3.4 Simulation with measurement data

When the physical experiments had been performed and the measurement data had been gathered and analysed, the system was simulated with the linear spring damper model. The aim was to recreate the physical measurements. The filtered torque measurement signal was used as input to the system and the response of the system was analysed. When a steady state solution had been found the result was calculated according to equation (3.5) - (3.6) as in the physical measurements.

In order to represent the real measurement values as closely as possible the stiffness and damping of the simulated system had to be adjusted. It was observed in the measurements that the amplitude of the torque due to the stiffness properties of the DMF rarely exceeded 750 Nm. This means that the stiffness first assigned, 9879 Nm/rad, was too high. The stiffness was changed to a lower value of 7813 Nm/rad. This value was calculated as the linear stiffness from 0 to 5.5° angular difference between the primary and secondary mass.

After the stiffness had been changed the damping coefficient in the simulation model could be altered to better represent the measured values. The cases listed in Table 3.3 were used to iteratively find a value of the damping coefficient before all cases were simulated. Only cases from the measurement without the clutch mounted was used to do these simulations. This was because the method was to find a damping coefficient for the case without the clutch. Then it should be checked if the same coefficient could be used when the extra inertia from the clutch was added to the system.

Table 3.3: The operating conditions used to iteratively find a value of the damping coefficient.

Speed	**Angle**
200 rpm	5°
400 rpm	7°
500 rpm	10°
600 rpm	5°
700 rpm	5°
800 rpm	10°
900 rpm	10°
1000 rpm	12°
1100 rpm	12°
1100 rpm	14°
1200 rpm	7°
1200 rpm	12°

The iterative process used was to simulate each case with a number of different values of the damping coefficient and calculate the amplitude of the speed fluctuations of the primary and secondary mass. The case with the smallest difference compared to the measured values was saved. This gave twelve different damping coefficients. After analysing the damping coefficient and the corresponding results the value for the damping coefficient was chosen to be 45 Nm/(rad/s). The chosen value for the damping coefficient was used to simulate all cases from the measurements, both with and without the mounted clutch. The results were then analysed and the loss in the simulated system could be calculated and compared to the measured values. To verify how well the amplitude of the speed oscillations of the primary mass had been calculated the simulation error was calculated as in equation (3.10) where $\omega_{p,m}$ and $\omega_{p,s}$ are the measured and simulated rotational speed of the primary mass.

$$Error = \frac{(\omega_{p,m} - \bar{\omega}_{p,m}) - (\omega_{p,s} - \bar{\omega}_{p,s})}{\omega_{p,m} - \bar{\omega}_{p,m}} \tag{3.10}$$

A damping coefficient depending on the torque input to the system would potentially give the possibility to give simulation results close to the measured values for a wider range of operating conditions. An attempt to find this was made but the time and available resources in this project proved to be too short to be able to do this with a quantitative result.

4 Results

4.1 Measurements

4.1.1 Dynamic behaviour

The dynamic behaviour of the DMF in the performed tests will be analysed in this section. The dynamics of the DMF will be studied as a function of mean rotational speed, Hooke's joint angle and if the clutch is mounted to the DMF or not.

The two input parameters to the test rig were the rotational speed and the angle of the propeller shaft. These two parameters were changed to get different levels of torque. In Figure 4.1 the amplitude of the measured torque is plotted as a function of the rotational speed. The two lines represent different angles of the Hooke's joint but both cases are with the clutch mounted. It can be seen that the torque amplitude is increasing with both rotational speed and Hooke's joint angle. This is also the expected result based on the theory presented in section 2.4.

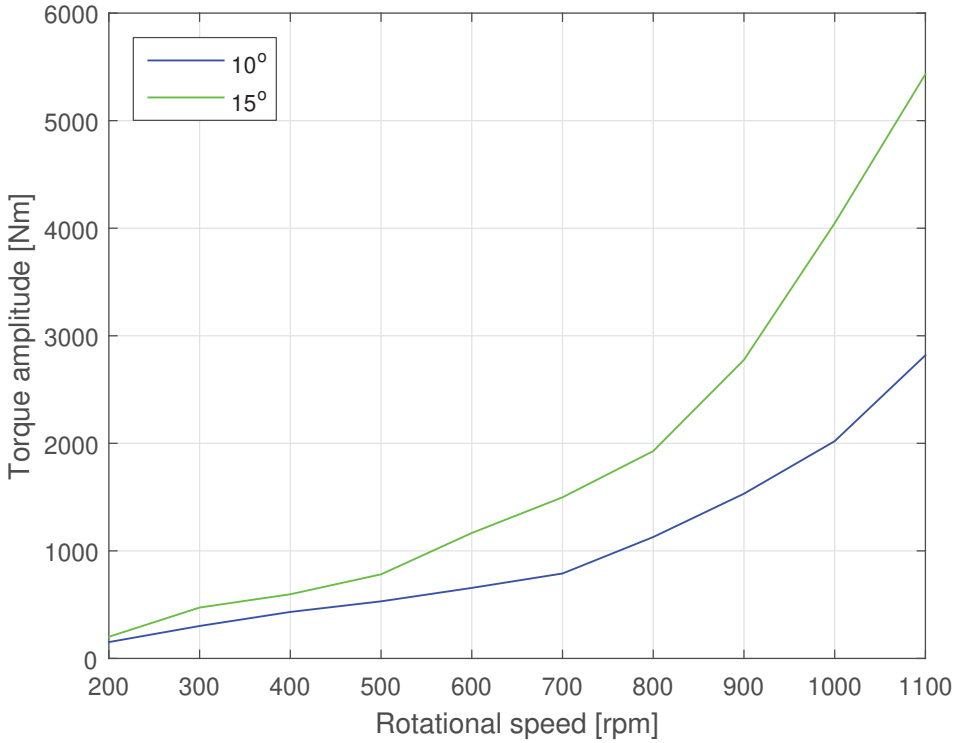

Figure 4.1: *Torque amplitude as function of rotational speed.*

If the speed of the primary and secondary mass is plotted against time for different mean rotational speeds the damping performance of the DMF can be analysed. In Figure 4.2 the speed of the primary and secondary mass is plotted against time for three different mean speeds with a Hooke's joint angle of 15° and without the clutch mounted. If the amplitude of the speed of the secondary mass is studied a clear difference between the three mean speeds can be observed. At 401 rpm the DMF is close to its resonance which can be seen by the fact that the amplitude of the speed is larger for the secondary mass than for the primary mass. When the mean speed is increased to 902 rpm the damping of the DMF can start to be observed. The secondary mass has a smaller amplitude than the primary mass. If the speed is increased further to 1103 rpm the damping of the speed fluctuations is clear. The amplitude of the secondary mass is about one third of the amplitude of the primary mass for this case. Another observation that can be made is that there is a phase difference between the primary and secondary mass. This phase difference is due to the inertial effects when the torque is transferred from the primary to the secondary mass via the springs.

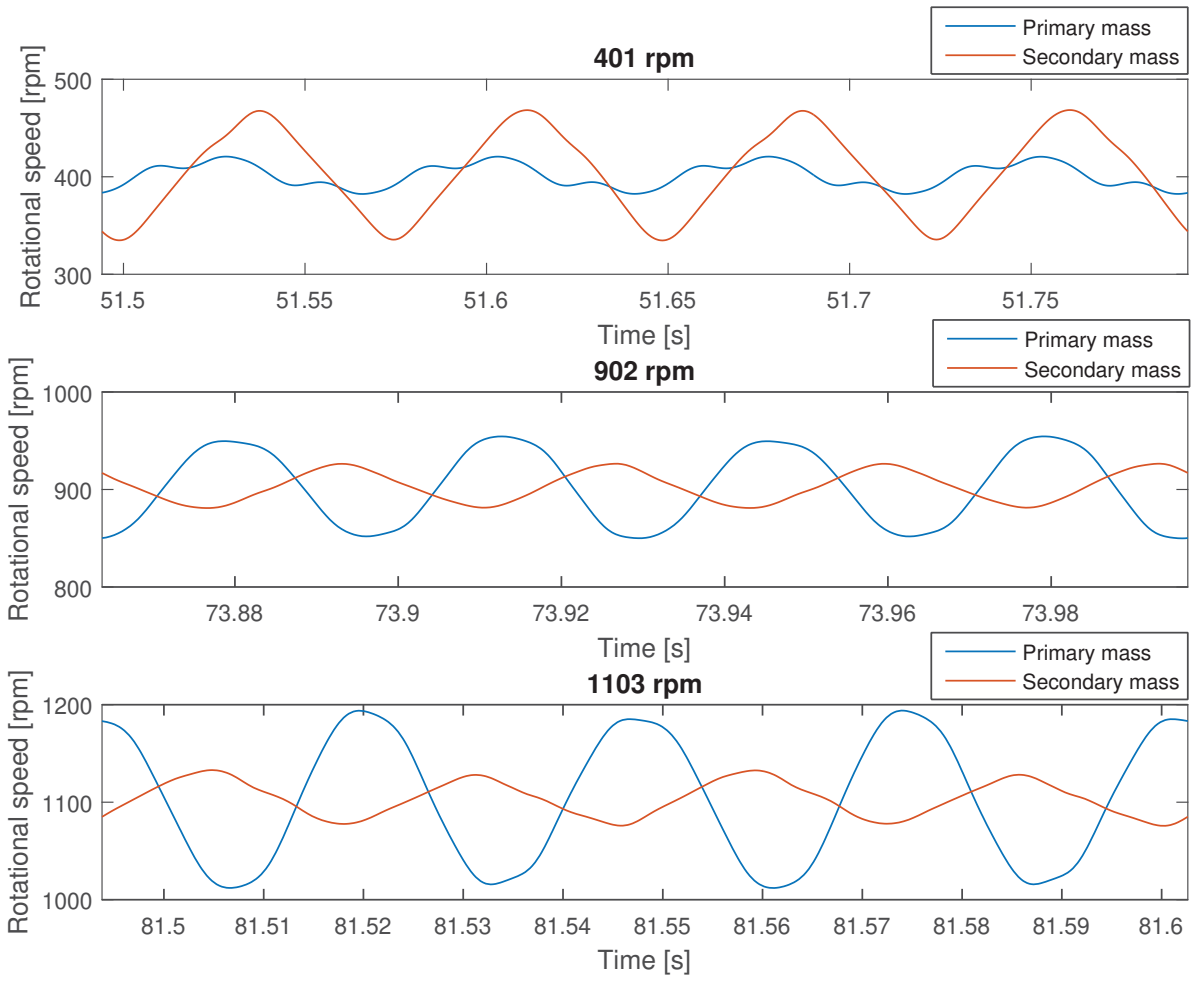

Figure 4.2: *Speed fluctuations of the primary and secondary mass for three different mean speeds, 15° Hooke's joint angle and without the clutch mounted.*

When the clutch is mounted to the DMF the inertia of the secondary mass is increased which changes the dynamic behaviour of the DMF. This can be observed by comparing Figure 4.2 with Figure 4.3. The plots displayed in Figure 4.3 are for the same operating points as in in Figure 4.2 but with the clutch mounted to the DMF. There is also a small change in the mean speed for one of the cases but this can be ignored since it is only one rpm difference. It can be seen that with a higher inertia the resonance is at lower speeds since at 401 rpm the speed fluctuations are starting to be damped out compared to the primary mass. An increased damping of the speed fluctuations can also be noted at the two higher mean speeds.

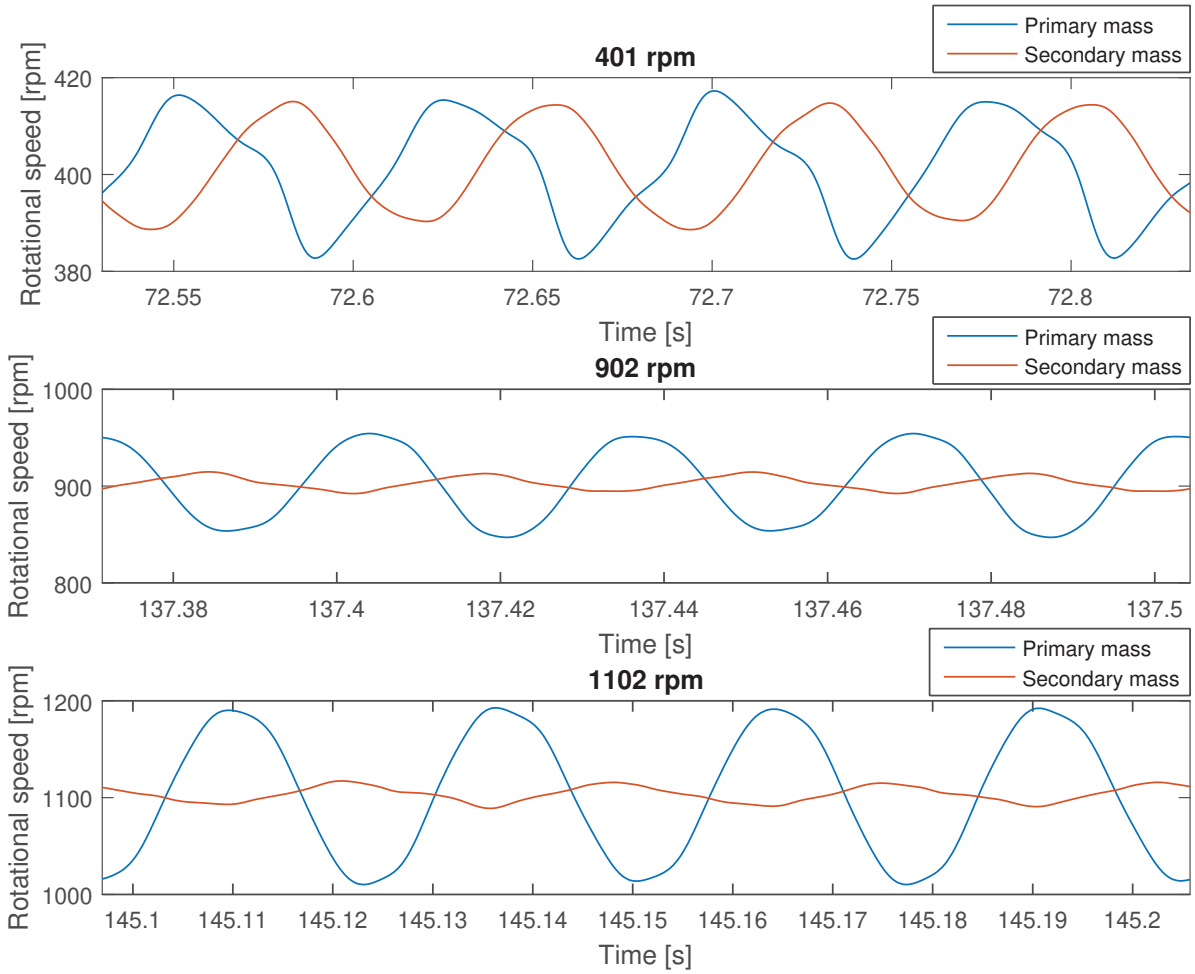

Figure 4.3: *Speed fluctuations of the primary and secondary mass for three different mean speeds, 15° Hooke's joint angle and with the clutch mounted.*

The difference in resonance speed can also be seen in Figure 4.4 where the amplitude of the speed fluctuations for the secondary mass is plotted against the rotational speed. It can be seen that for the case where there is no clutch mounted there is a resonance at approximately 400 rpm. This resonance is lowered to approximately 300 rpm when the clutch is mounted. Another observation that can be made is that the resonance seems to depend on the angle of the Hooke's joint. For the case without the mounted clutch there is a clear difference between the three angles. The reason for this is likely to be that the mechanical properties of the propeller shaft changes when the joint angle is changed due to internal clearance or non linear stiffness in the joint. This means that the resonance speed for the whole system is changed. A third observation is that the amplitude is lower for the case where the clutch is mounted. This is probably due to the fact that the torque input to the system increases with rotational speed as can be seen in Figure 4.1. This means that for a resonance at lower speeds the torque input is lower and thus the amplitude of the speed fluctuations will be lower.

If Figure 4.4 is compared to Figure 3.12 and 3.13 it can be noted that the first simulations predicted the resonance speeds well. The amplitude of the speed oscillations was too high in the simulations which indicates that the damping coefficient is higher in reality than what was used in the simulations before the measurements.

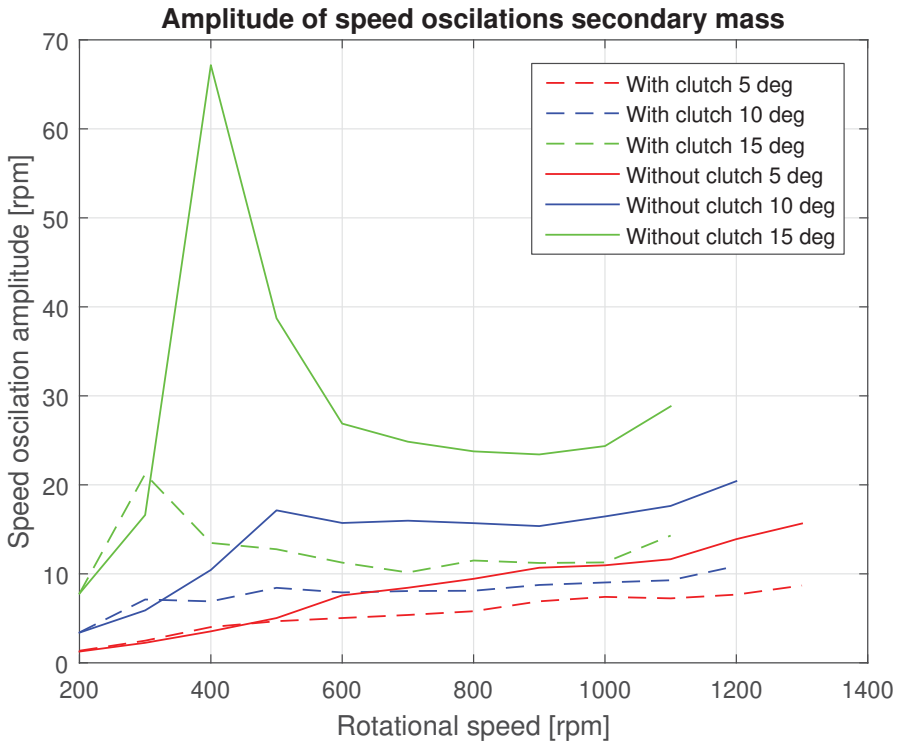

Figure 4.4: *Amplitude of the speed oscillations of the secondary mass for three different angles of the Hooke's joint.*

In Figure 4.5 the measured torque is plotted against rotational speed for three different Hooke's joint angles and for both the case with and without the clutch mounted. It can be seen that adding extra mass and thereby extra inertia to the secondary mass does not increase the torque significantly. The reason for this can be found by studying Figure 4.2 - 4.3. It can first be observed that the speed fluctuations are lower for the secondary mass than for the primary mass except where there is a resonance. This means that the acceleration will also be lower which in turn means lower torque according to Newton's second law. It can also be noted that when the clutch is attached the speed fluctuations of the secondary mass are damped more than for the case where the clutch is not attached. Combining these two observations concludes that adding extra inertia to the secondary mass will not have a large impact on the torque amplitude. This is because the speed fluctuations are damped and thus the acceleration levels are lower as well except for where there is a resonance peak in the speed fluctuations of the secondary mass. If Figure 4.5 is studied this is also what can be seen. At low speeds, near the resonance speed, for the case with the clutch mounted the torque levels are a bit higher than without the extra inertia of the clutch. At higher speeds the damping action of the DMF will reduce the impact of the higher inertia and no significant difference can be seen.

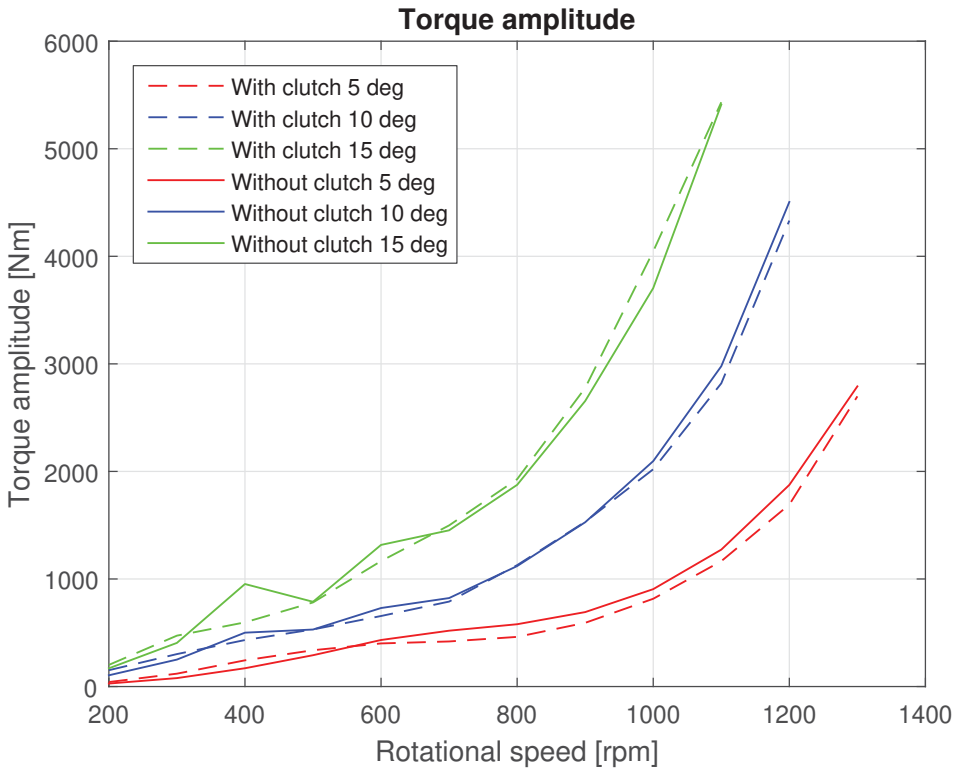

Figure 4.5: *Amplitude of the measured torque for three different angles of the Hooke's joint.*

4.1.2 Friction losses

The losses were calculated as shown in equation (3.5). If the loss for the case without the clutch attached is plotted against the maximum speed difference between the primary and secondary mass, the plot in Figure 4.6 is obtained. It can be seen that the loss is increasing with increased speed difference. It can also be noted that the mean speed, which is represented by the different colours, does not seem to affect the loss. This indicates that the losses primarily originates from viscous friction. The plot shows no direct relationship between input torque amplitude and loss but a higher torque amplitude at a fixed mean speed will give a larger speed difference between the primary and secondary mass which means higher losses.

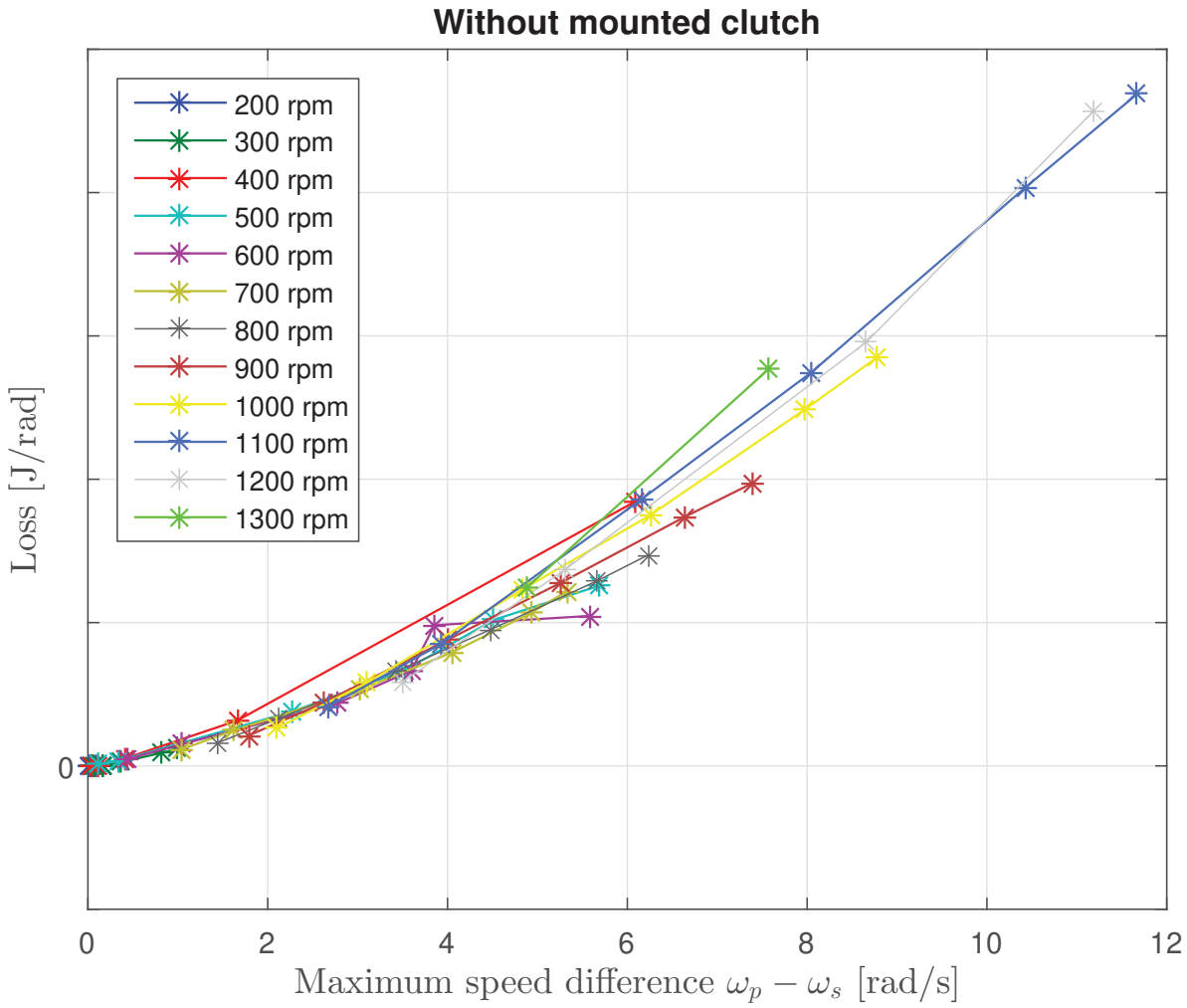

Figure 4.6: *Loss as function of maximum speed difference between the primary and secondary mass for the measurements without the clutch mounted to the secondary mass.*

In Figure 4.7 the losses with the clutch mounted to the secondary mass is plotted against the maximum speed difference. The scale of both the x- and the y-axis are the same as in Figure 4.6. The trend is the same as for the case without the clutch but the inclination of the curve is steeper for the case with the mounted clutch. This is probably due to the extra torque required to rotate the larger inertia which will give higher losses for a given speed difference.

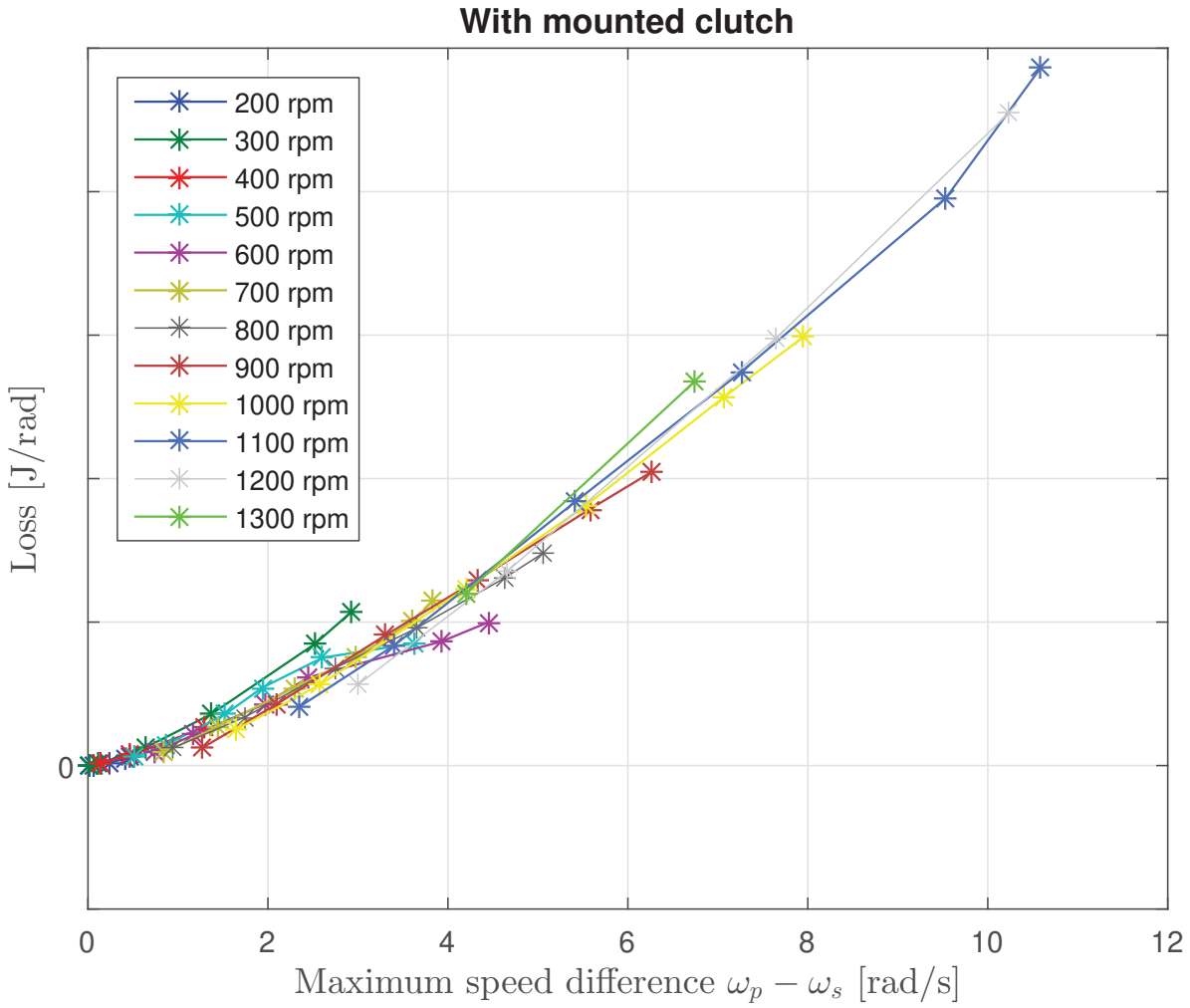

Figure 4.7: *Loss as function of maximum speed difference between the primary and secondary mass for the measurements with the clutch mounted to the secondary mass.*

The uncertainty of the torque sensor is considered in Figure 4.8 - 4.9 where the losses are plotted against the maximum possible speed difference between the primary and secondary mass. The lines with o markers represent the maximum positive error while the lines with Δ markers are the maximum negative error. As can be seen they are close to the original plot (star markers) which means that the error from the torque sensor is small and will be neglected in the results from this point.

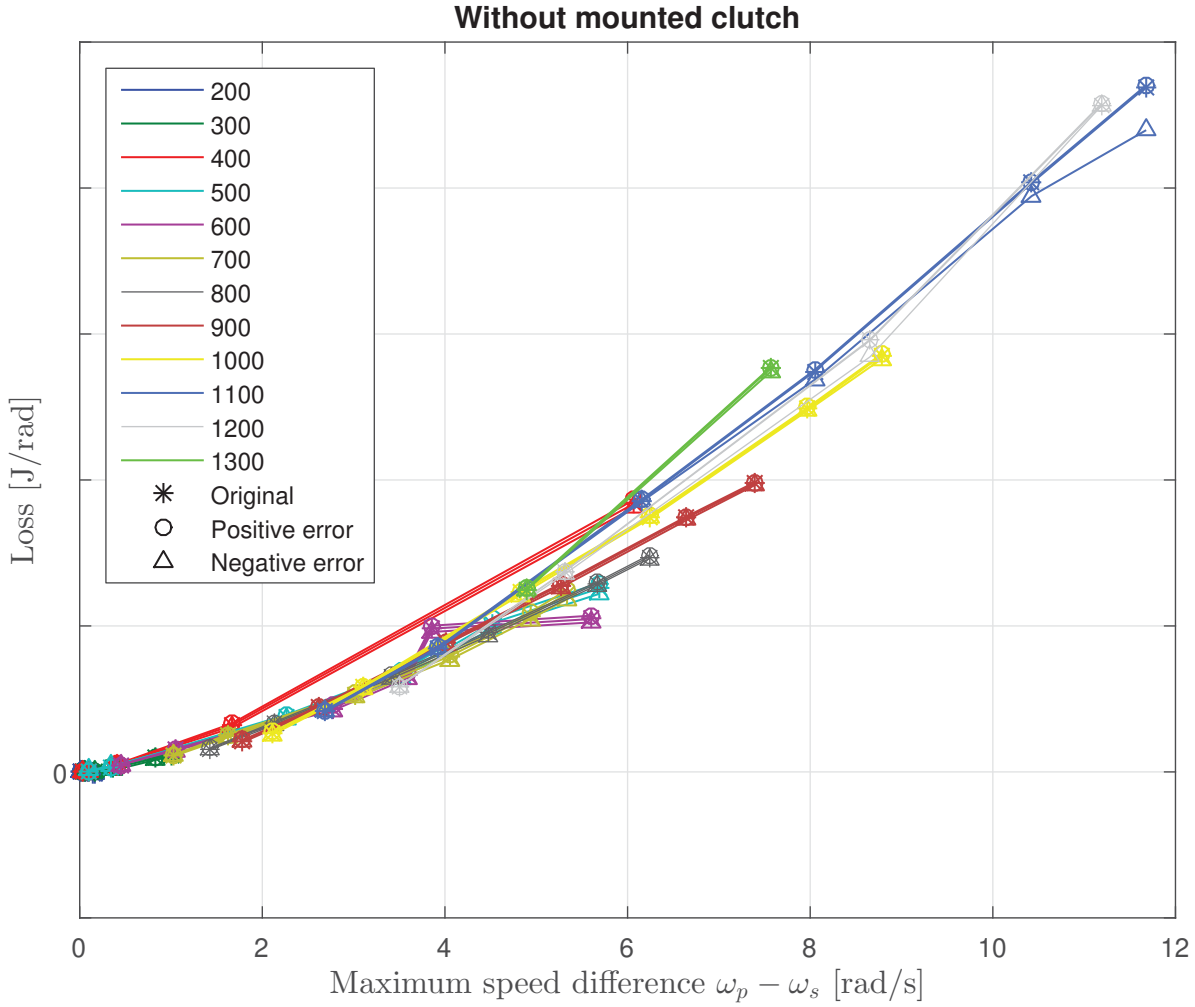

Figure 4.8: *Loss as function of maximum speed difference between the primary and secondary mass with the uncertainty of the torque sensor for the measurements without the clutch mounted to the secondary mass.*

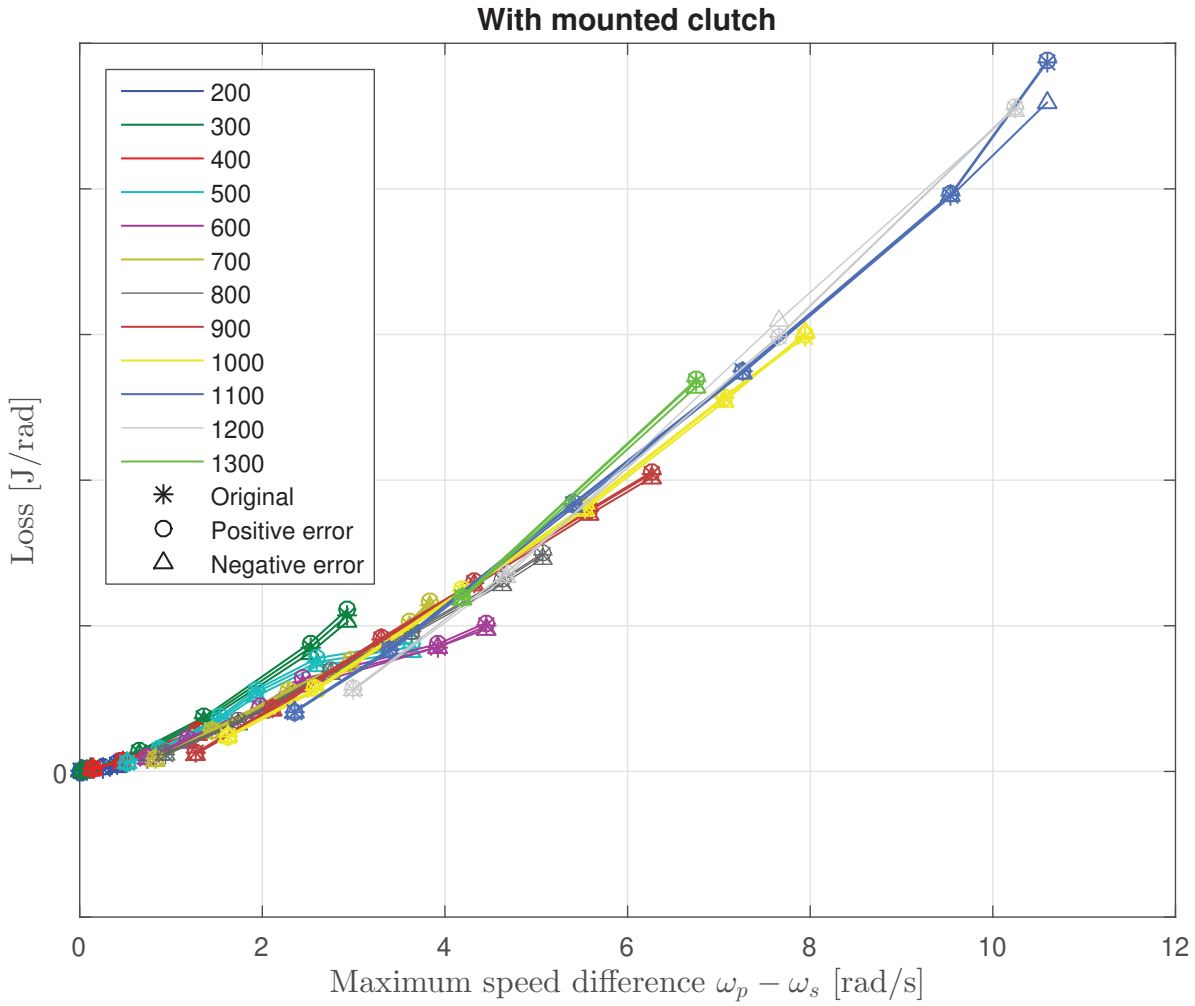

Figure 4.9: *Loss as function of maximum speed difference between the primary and secondary mass with the uncertainty of the torque sensor for the measurements with the clutch mounted to the secondary mass.*

4.2 Simulation

By using the iterative process described in section 3.3.4 a good value for the damping coefficient for the case without the clutch mounted was found to be 45 Nm/(rad/s). The results from the simulations with this value of the damping coefficient for the case where the clutch is not mounted can be seen in Figure 4.10 where the loss is plotted as a function of maximum speed difference between the primary and secondary mass. The red dots indicate the measured loss and the black dots indicate the simulated loss. It can be seen that the overall trend is the same for both the measured and the simulated loss. However it can also be seen that each specific case does not match as well as the overall trend. It can thus be said that to get an understanding of how the loss will behave as a function of the speed difference between the two masses the simulation model works well. If the aim is to get the exactly correct loss for one specific operating point the simulation model will not perform as well.

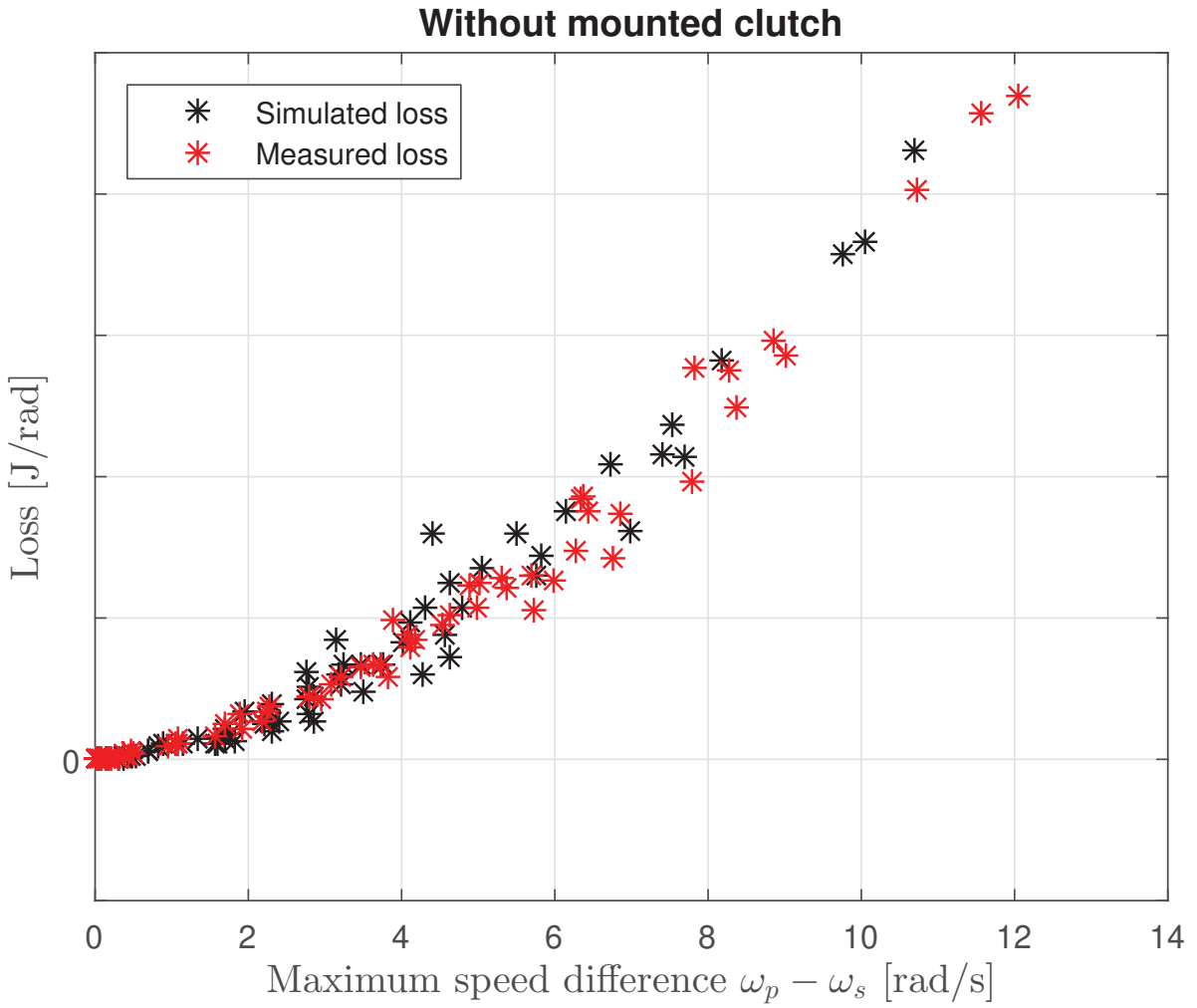

Figure 4.10: *Loss as function of maximum speed difference between the primary and secondary mass for the measurements and simulations without the clutch mounted to the secondary mass.*

The reason why each specific operating point does not match well between the measurements and the simulations is that the amplitude of the primary mass is not correct from all simulations. As can be seen in equation 3.5, which was used to calculate the loss, the only two variables are the torque and the speed of the primary mass. Since the torque was the the same for both the measurements and the simulation the only varying parameter is the speed of the primary mass which is why this is the source of the error. In Figure 4.11 the error of the simulated amplitude of the speed of the primary mass can be seen for all measured and simulated angles of the Hooke's joint. As can be seen the error is varying and is as large as -63% for one operating point. This is the reason why all operating points do not match well between measurements and simulation. It can also be seen that a majority of the operating points are within $\pm 10\%$ error which is why the overall trend matches well between the measurements and the simulations. The large errors at 500 rpm can be explained by that there is a resonance in the simulation model at around this speed. This is why the amplitude is overestimated at this speed. The reason why all simulated cases at this speed are not following this trend has not been found.

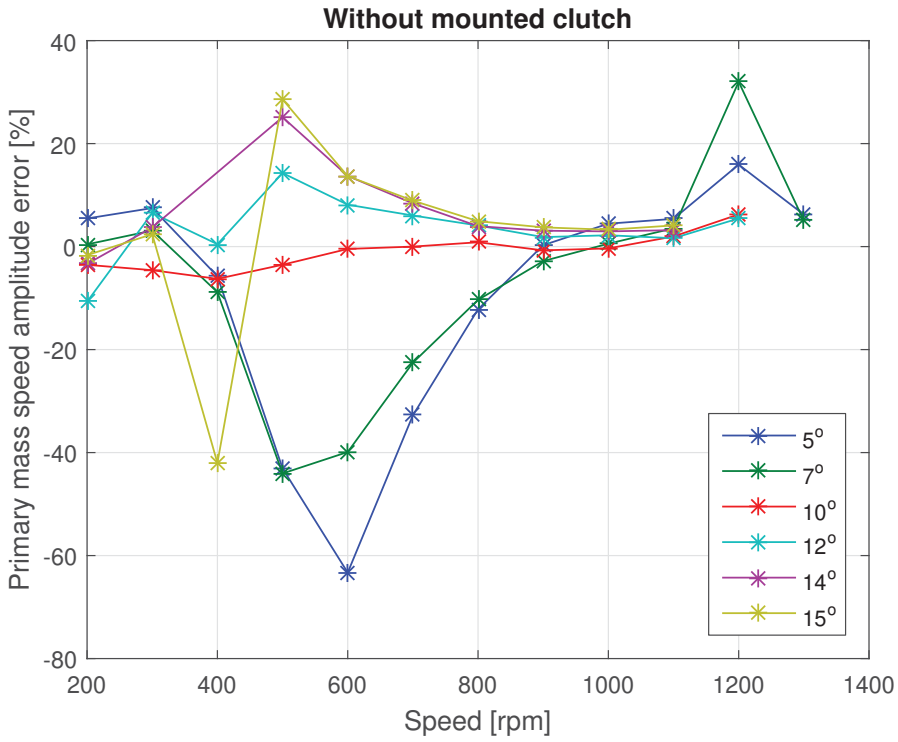

Figure 4.11: *Amplitude error of the speed of the primary mass for all measured and simulated angles of the Hooke's joint.*

If the simulation model is used to predict the losses when the clutch is mounted to the secondary mass the result is not as good as for the case without the mounted clutch. The calculated and measured loss as a function of maximum speed difference between the primary and secondary mass can be seen in Figure 4.12. As can be seen the shape of the curve for the simulated losses matches the measured data well but the simulated losses are consequently lower than the measurements. The error is however small except at speed differences of around 4 rad/s. The problem that the loss for each specific case does not match between the measurements and the simulations remains from the case without the clutch mounted.

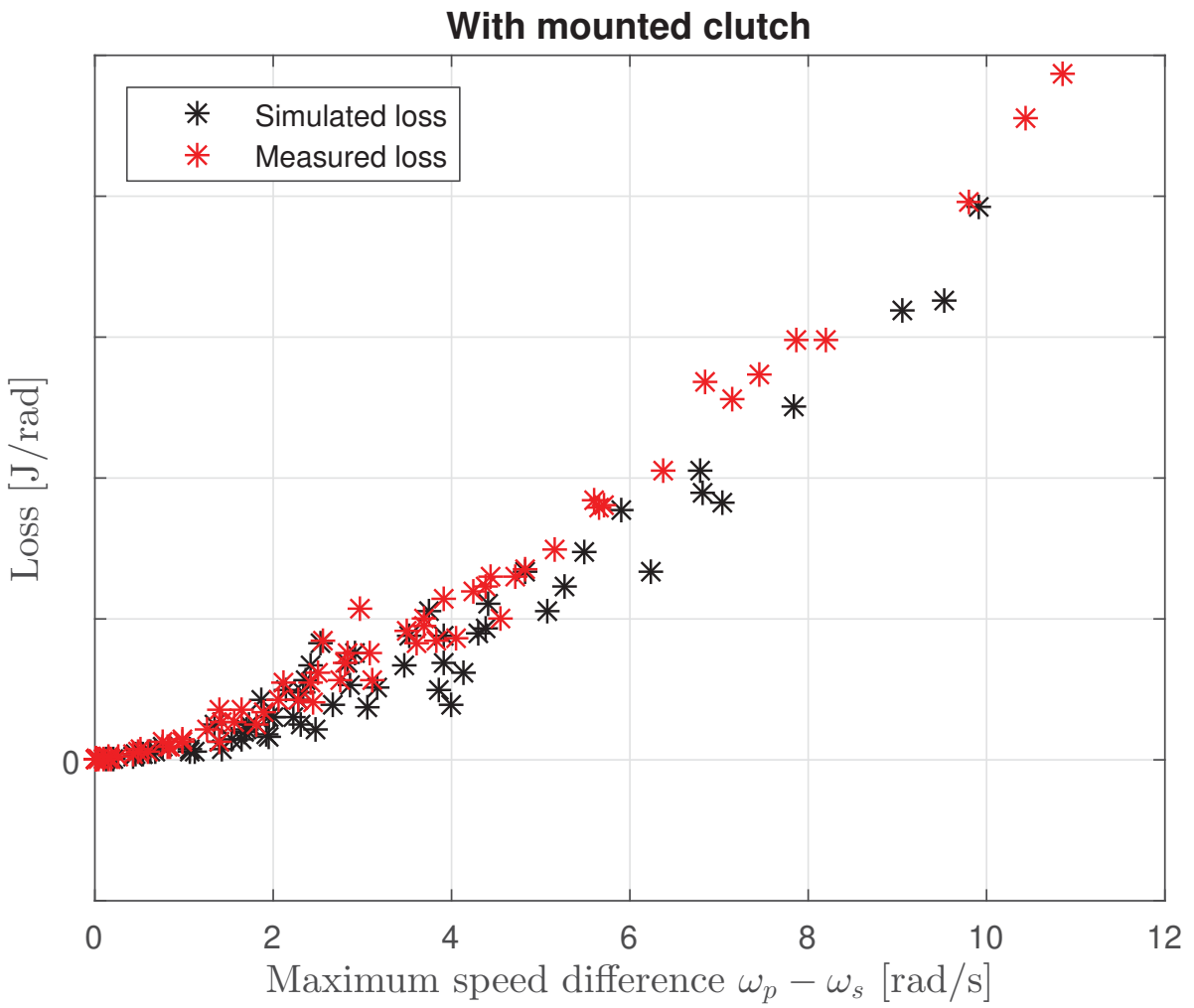

Figure 4.12: *Loss as function of maximum speed difference between the primary and secondary mass for the measurements and simulations with the clutch mounted to the secondary mass.*

The reason for the large deviation at speed differences of around 4 rad/s can be explained by studying Figure 4.13. There, the error of the simulated amplitude of the speed of the primary mass can be seen for all measured and simulated angles of the Hooke's joint. It can be seen that there are large errors at 400-600 rpm for the smaller angles. This is the area that corresponds to the speed difference where the error is large. The resonance in the simulation model for the case with the mounted clutch is at approximately 400 rpm. This is the reason why the simulated amplitude is overestimated at this point. Since the measured amplitudes of the speed oscillations are increasing with the joint angle the largest percentage error will occur at the smallest joint angle.

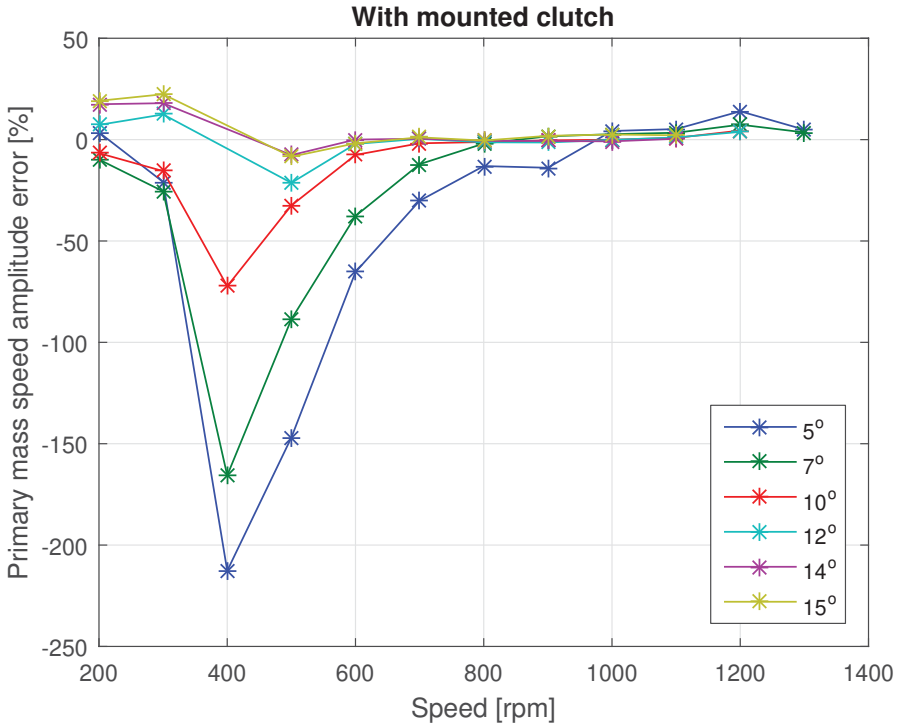

Figure 4.13: *Amplitude error of the speed of the primary mass for all measured and simulated angles of the Hooke's joint.*

5 Discussion

When doing measurements and analysing the data gathered from these measurements there are several possible sources of error and the major ones will be discussed in this section. A critical analysis of the performed simulations will also be made and possible improvements will be discussed. Finally an overall conclusion on how well the sources of error were dealt with will be made.

Firstly one general point that should be made is concerning the operating points during the measurements and thus also during the simulations. Because of how the test rig is constructed it was only possible to have a torque input that oscillated around zero. This is not the case in a real truck where there is instead a positive mean torque at drive and the torque is fluctuating around this. This means that there is a difference in spring deflection between the measurements and real driving which in it turns means that different parts of the springs are active between the measurements and real driving. A finding in the measurements was that the viscous friction is dominating which means that the level of deflections in the springs should not affect the results significantly. It can however not be concluded that it will not have an effect. Therefore it would be interesting to do measurement either in a real truck or in a test rig that is able to apply a braking torque to the secondary mass.

The largest source of error in the measurements in this project is the temperature of the grease in the DMF. As has been discussed in previous sections the temperature of the grease affects the friction properties of the DMF and it is therefore of interest to keep this temperature as stable as possible. The source of error in the measurements is that the temperature of the grease was not measured. Even though the temperature of the surrounding material was measured and proved to be stable throughout all measurements there is no guarantee that the temperature of the grease was equally stable. One way of verifying that the properties of the grease has been stable is by doing measurements of the same operating point separated in time which was the method used in this project. Measurements at steady state speed of 700 rpm with the same angle of the Hooke's joint were performed at separated times and with other steady state speeds ran in between the measurements. The results were similar and no clear difference could be observed between the two measurements. This indicates, along with the temperature measurements, that the temperature of the grease was stable throughout the measurements.

Due to the limited time available for measurements in the project, each point of measurement was measured only once (except for the tests to verify that the temperature of the grease had been stable). This means that the repeatability of the measurements was not addressed. The probability that the results should not be repeatable is however judged to be small since the system used is purely mechanical and therefore should not change significantly over time.

Another source of error lies in the analysis of the measured data. When calculating the losses two assumptions were made. Firstly that all losses originated from the friction in the DMF and secondly that the adapters between the torque sensor and the DMF were completely rigid. The first assumption is correct apart from that there is a bearing that supports the input shaft to the sleigh that is not completely loss free. There is however no way of measuring the torque after this bearing and calculations of losses in bearings are outside the scope of this project. Therefore this source of error will have to be accepted. The second assumption is most probably correct enough to be able to neglect the possible error. The stiffness of the adapters between the torque sensor and the DMF are known and the maximum measured torque gives a neglectable deflection angle. This means that there is no significant time difference between a measured torque and the corresponding speed of the primary mass.

One possible error is that the measured signals have been affected by disturbances. These types of disturbances can for example be an electric or magnetic field. Even though there probably are disturbances of this kind in the test cell, for example from the electric motor driving the rig, it has most probably not affected the measurements. This can be said since shielded wires were used for all speed signals as well as for the torque signal. Other possible disturbances like measurement noises were dealt with by using an anti-aliasing filter in the data acquisition system.

The calculation of the torque sensor error is another source of error. All factors concerning calibration parameters were omitted as well as the parameter based on experience. Omitting these factors can lead to an underestimation of the error in the sensor. This is also the case for the parasitic loads and the temperature dependent parameters. To avoid this the parasitic loads and the temperature difference in the sensor were estimated with high safety margins. Thus, the calculated value is probably worse than the real error for these factors.

The largest error concerning the simulations originates from the stiffness used. If the stiffness curve in Figure 2.4 in section 2.2 is studied it can be seen that is has three different inclinations depending on the level of angle difference between the primary and the secondary mass. Depending on the operating conditions the angle difference in this project has been changing between the first and the second inclination. In the simulations only one value of the stiffness has been used. This value was calculated before the simulations were performed by analysing the measured data. It would perhaps have been a better method to try to optimise both the stiffness and the damping coefficient in the model rather than just the damping coefficient which was what was done.

When the damping coefficient of the simulation model was selected the objective was to simulate the amplitude of the speed oscillations of the primary mass as close as possible compared to the measured values. This was done to be able to simulate the losses as well as possible. No consideration was taken to how well the total dynamic behaviour of the simulation model matches the measured values. This was not evaluated either. It would potentially be possible to find a damping coefficient with which both the dynamic behaviour and the losses are simulated with satisfying results.

As mentioned in section 3.3.4 the time was too short to be able to find a damping coefficient as a function of the torque input. If this had been done it would potentially increase the accuracy in the simulated results. It could give the potential to simulate specific operating points with accurate results and not just the overall behaviour as is the case with the fixed damping coefficient used in this project.

To summarise it can be said that there are some possible sources of error. Most of them have been dealt with in the best way possible within this project and some of them just have to be accepted or are so small that they can be neglected. The measured data have been stable, reliable and trustworthy throughout the project which is why the conclusion can be drawn that the possible errors have not affected the outcome of the project significantly.

6 Conclusions

In this project both measurements and simulations of the dynamic friction losses in a DMF for commercial vehicles have been performed. Both measurements and simulations have been performed with two levels of inertia at the secondary mass, with and without a mounted clutch. In the measurements a varying torque and speed input was created by using a propeller shaft with a Hooke's joint. Since no brake torque was applied to the DMF this creates a torque oscillating around zero. The input to the system was the rotational speed and the angle of the Hooke's joint. The torque after the Hooke's joint was measured and then used as input to the simulation model.

The measured data has been stable throughout the measurements and the temperature of both the DMF and the surrounding air has been controlled and proved stable. The losses in the DMF have been simulated with a linear spring damper model with constant values for the spring and damping coefficient. With the right numerical value of the damping coefficient the simulated and measured results are similar.

Both the results from the measurements and the simulations indicate that the friction in the DMF is primarily viscous. Thus, the losses in the DMF are primarily dependent on the speed difference between the primary and secondary mass. This trend is valid for both the case with and without the clutch even though the losses are larger with the clutch mounted to the secondary mass. Neither a direct relation between the losses and mean rotational speed nor between the losses and the torque amplitude could be seen.

As further research it suggested that measurements with a constant mean torque and a torque oscillating around this are performed to better recreate the conditions from a real driving scenario. For the simulation part it is suggested to try to find a damping coefficient that is dependent on the torque input to the system. This would potentially increase the accuracy of the simulated results.

Bibliography

[1] Volvo trucks image and film galery. `http://images.volvotrucks.com`. Accessed: 2018-05-02.

[2] Heinz Heisler. *Vehicle And Engine Technology*. Elsevier Ltd., second edition, 1999.

[3] P Kelly, B Pennec, R Seebacher, B Tlatlik, and M Mueller. Dual mass flywheel as a means of attenuating rattle. In *Tribology and Dynamics of Engine and Powertrain*, pages 857–877. Elsevier, 2010.

[4] LUK. *Dual Mass Flywheel - Special Tool User Instructions*.

[5] S Theodossiades, M Gnanakumarr, H Rahnejat, and P Kelly. Effect of a dual-mass flywheel on the impact-induced noise in vehicular powertrain systems. *Proceedings of the Institution of Mechanical Engineers, Part D: Journal of Automobile Engineering*, 220(6):747–761, 2006.

[6] Ad Kooy, Achim Gillmann, Johann Jäckel, and Michael Bosse. Dmfw - nothing new. In *7th LuK symposium*, pages 5–14, 2002.

[7] U.Schaper, O. Sawodny, T. Mahl, and U. Blessing. Modeling and torque estimation of an automotive dual mass flywheel. In *2009 American Control Conference*, pages 1207–1212, June 2009.

[8] Lei Chen, Rong Zeng, and Zhengfeng Jiang. Nonlinear dynamical model of an automotive dual mass flywheel. *Advances in Mechanical Engineering*, 7(6), 2015.

[9] ZF Sachs. Drawing number: 326594000058. Technical Drawing, 2005.

[10] E. Galvagno, A. Tota, M. Velardocchia, and A.Vigliani. Test bench characterisation and frequency domain torsional model validation of transmission systems and components. In *TrC-IFToMM Symposium on Theory of Machines and Mechanisms*, June 2015.

[11] E. Galvagno, M. Velardocchia, A. Vigliani, and A. Tota. Experimental analysis and model validation of a dual mass flywheel for passenger cars. *SAE Technical Paper 2015-01-1121*, 2015.

[12] Tobias Mahl and Oliver Sawodny. Modelling of an automotive dual mass flywheel. *IFAC Proceedings Volumes*, 43(18):517 – 523, 2010. 5th IFAC Symposium on Mechatronic Systems.

[13] Bernd Sauer and Andreas Nicola. Rotational vibrometers help determine the transmission behavior of a dual mass flywheel. *Polytec InFocus 1/2007*, 2007.

[14] Henrik Ryberg. ER-600130. Technical report, Volvo Powertrain Corporation, April 2004.

[15] Henrik Ryberg. ER-600729. Technical report, Volvo Powertrain Corporation, August 2004.

[16] Hans Kask. ER-221878. Technical report, Volvo Powertrain Corporation, October 2002.

[17] Gérémy Bourgois. Dual mass flywheel for torsional vibrations damping. Master's thesis, Chalmers University of Technology, 2016.

[18] Daniel Johansson and Kim Karlsson. Simulation models of dual mass flywheels. Master's thesis, Chalmers University of Technology, 2017.

[19] Andreas Walter, Uwe Kiencke, Stephen Jones, and Thomas Winkler. Misfire detection for vehicles wih dual mass flywheel (dmf) based on reconstructed engine torque. In *Asia Pasific Automotive Engineering Conference*. SAE International, August 2007.

[20] Albert Albers, Marc Albrecht, Arne Krüger, and Ralph Lux. New methodology for power train development in automotive engineering - integration of simulation, design and testing. In *Automotive and Transportation Technology Congress and Exposition*. SAE International, October 2001.

[21] Mart Mägi and Kjell Melkersson. *Lärobok I Maskinelement*. EcoDec International AB, 2006.

[22] Bengt Sundström and Instutionen för hållfasthetslära Kungliga Tekniska Högskolan. *Handbok och formelsamling i Hållfasthetslära*. Instutitionen för hållfasthetslära, KTH, 1998.

[23] M.M. Japp. Formelsamling i mekanik, September 2003.

[24] Roy R Craig and Andrew J Kurdila. *Fundamentals of structural dynamics*. John Wiley & Sons, 2006.

[25] Nathan M. Newmark. *Computation of dynamic structural response in the range approaching failure*. Department of Civil Engineering, University of Illinois, 1952.

[26] Siemens PLM Software. *Identifying best practices for measuring and analyzing torsional vibration*. Siemens, 2014.

[27] Georg Wegener and Jürgen Andrae. Measurement uncertainty of torque measurements with rotating torque transducers in power test stands. *Measurement*, 40(7):803 – 810, 2007.

[28] Hottinger Baldwin Messtechnik GmbH. T12 digital torque transducer data sheet.

Appendix A Measurement uncertainty

Here, the parameters needed to calculate the uncertainty of the measurements according to [27] will be presented and the numerical values of the parameters used will be listed. As described in section 2.7.2 all parameters were not known and therefore some of them were omitted in the calculations. In Table A.1 the parameters are listed along with the numerical values of the parameters used. The specification of the torque sensor is listed in Table A.2. All numerical values are taken from [28].

Table A.1: Parameters for calculations of measurement uncertainty of the torque signal.

Parameter	**Available from**				**Numerical value**
	Data sheet	*Test Protocol*	*Calibration*	*Experience*	
TK_0	x				± 0.02%
TK_C	x				± 0.03%
d_{lh}	x	x			± 0.006 - ± 0.02% [1]
σ_{rel}	x		x		± 0.01%
b			x		-
d_c			x		-
f_{rem}			x		-
d_{para}	x		x		± 0.3%
d_{speed}				x	-

[1] This parameter is dependent on the applied torque.

Table A.2: The specification of the torque sensor.

Product name	HBM T12 10 kNm
Nominal rated torque (M_{nom})	10 kNm
Nominal rated speed (n_{nom})	10 000 rpm
Accuracy class	0.03
Calibration date	2018-01-23

The calculated individual contributions and total uncertainties can be seen in equation (A.1) - (A.6). To calculate the contribution U_p the parasitic loads on the torque sensor had to be estimated. They were estimated to be approximately 1% of the allowed longitudinal load, 5% of the allowed lateral load and 25% of the allowed bending torque. In [27] a value of 1 for the constant k is suggested when using parameter values from the datasheet of the sensor and this was used in the calculations in this project. The temperature difference in the sensor was estimated to have been maximum 5 Kelvin.

$$U_{TK0} = M_{nom} TK_0 \frac{\Delta T}{10K} = 10000 \cdot 2 \cdot 10^{-4} \cdot \frac{5}{10} = 1 \ Nm \tag{A.1}$$

$$U_{TKC} = M_{ap} TK_C \frac{\Delta T}{10K} = M_{ap} \cdot 3 \cdot 10^{-4} \cdot \frac{5}{10} = M_{ap} \cdot 1.5 \cdot 10^{-4} \tag{A.2}$$

$$U_{lh} = M_{nom} d_{lh} = \begin{cases} \max & 10000 \cdot 2 \cdot 10^{-4} = 2 \ Nm \\ \min & 10000 \cdot 6 \cdot 10^{-5} = 0.6 \ Nm \end{cases} \tag{A.3}$$

$$U_{b'} = k \frac{M_{ap}}{\Delta M_{ref}} \Delta M_{ref} \sigma_{rel} = M_{ap} \cdot 10^{-4} \tag{A.4}$$

$$U_p = M_{nom} d_{para} \frac{L_{para}}{L_{para,ref}} = 10000 \cdot 3 \cdot 10^{-3} \cdot \frac{31}{100} = 9.3 \ Nm \tag{A.5}$$

$$U = \sqrt{U_{TK0}^2 + U_{TKC}^2 + U_{lh}^2 + U_{b'}^2 + U_p^2} \tag{A.6}$$

Appendix B Test set up and drawings

Here, a list is presented of all components used in the test set up along with a wiring scheme and drawings of the adapters designed and manufactured during the project. In Table B.1 all components from the test set up are listed along with some important parameters. The stiffness of the DMF is non linear which is why it is not listed. The propeller shaft is a custom made part for the rig used in the measurements and no drawing or part number exist. Its mechanical properties were estimated from drawings of other propeller shafts. The adapters used are also specially built and thus do not have a part number. The stiffness of the clutch disc and the pressure plate is not of interest for the measurements which is why that property is not listed.

Table B.1: The used parts in the test set up and some important parameters.

Part name	**Volvo prt. no.**	**Mass [kg]**	**Moment of inertia [kgm^2]**	**Stiffness [Nm/rad]**
DMF	SACHS 326594000205	82	$J_p = 1.8$ $J_s = 0.9$	-
DMF-adapter	21260833	1.56	0.007	$3.27{\cdot}10^7$
Clutch disc	22442367	Classified	Classified	-
Pressure plate	21648792	Classified	Classified	-
Propeller shaft	-	42	0.14	$3.56{\cdot}10^5$
Adapter 1	-	16	0.18	$4.19{\cdot}10^8$
Adapter 2	-	19	0.11	$1.65{\cdot}10^7$
Adapter 3	-	23	0.37	$2.63{\cdot}10^9$
Adapter 4	-	19	0.21	$2.49{\cdot}10^7$

In Table B.2 the sensors used are listed and the wiring scheme is presented in Figure B.1. As can be seen in the wiring scheme a common ground was used for the whole system. The wires used for the speed, torque and surface temperature measurements were shielded to avoid disturbances in the measured signal.

Table B.2: The used sensors in the test set up.

Measurement	**Sensor model**
Torque	HBM T12HP 10 kNm
Angular speed primary mass	Classified
Angular speed secondary mass	TTI LT-880
Test rig speed	Classified
Surface temperature	Optris CT LT20
Logging of DMF temperature	MSR145
Acceleration rig base	PCB 356B20
Acceleration torque sensor	PCB 356B20
CAN acquisition	AD-Scan Mini Modul
CAN temperature acquisition	Termo-Scan Mini Modul
Data acquisition system	DEWESoft SIRIUS

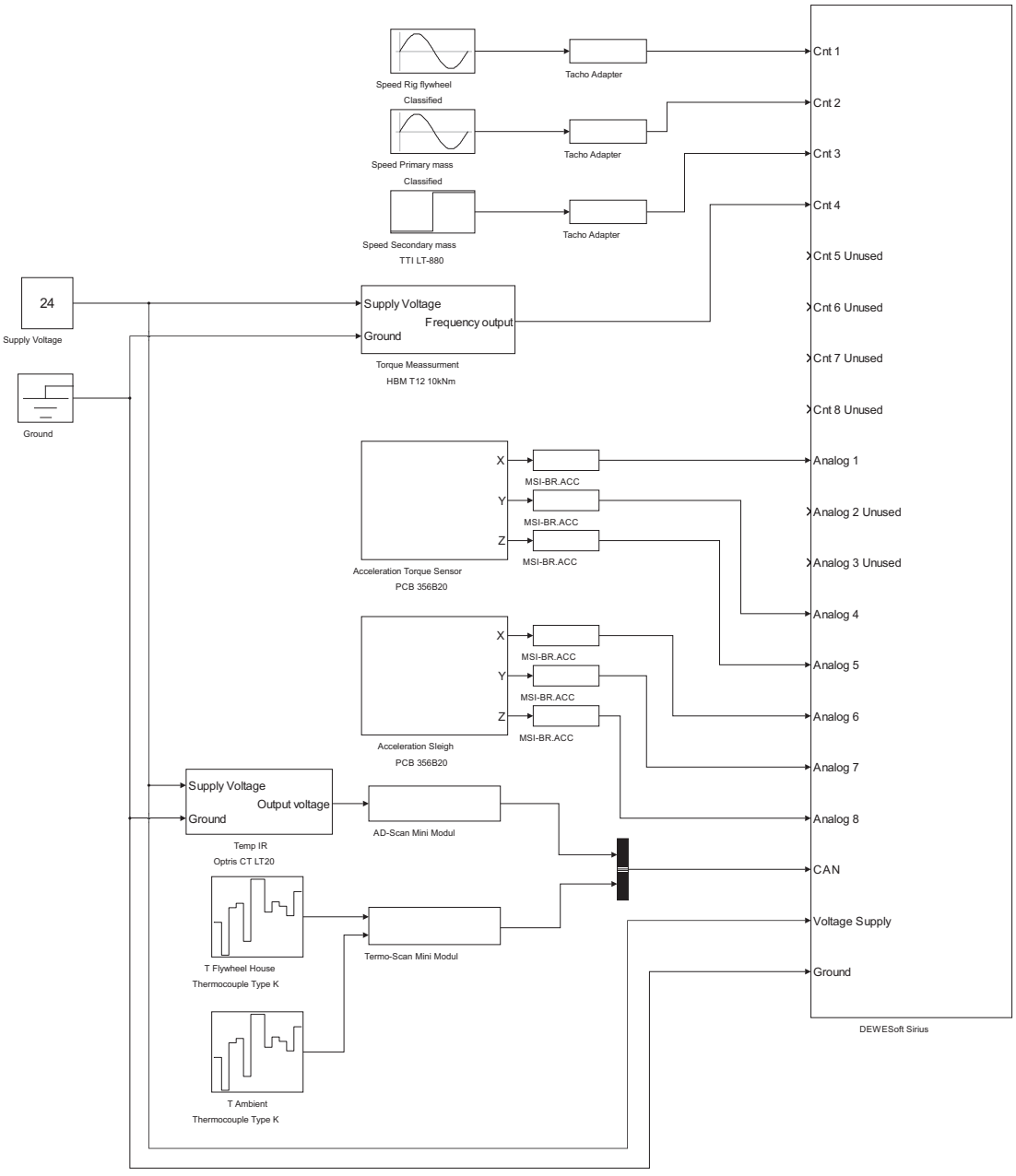

Figure B.1: *Wiring scheme of the sensors used in the measurements.*

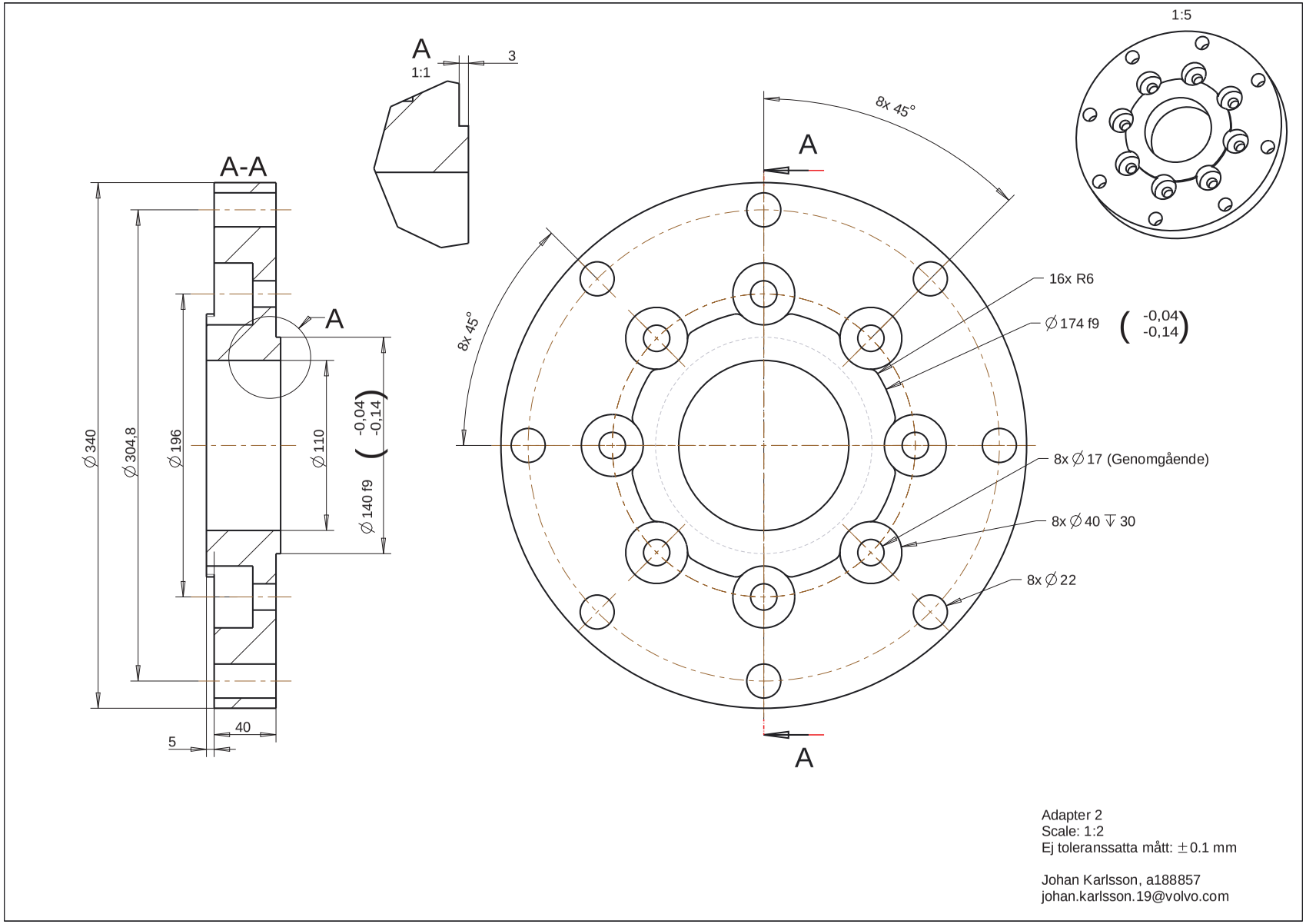

Adapter 2
Scale: 1:2
Ej toleranssatta mått: ±0.1 mm

Johan Karlsson, a188857
johan.karlsson.19@volvo.com

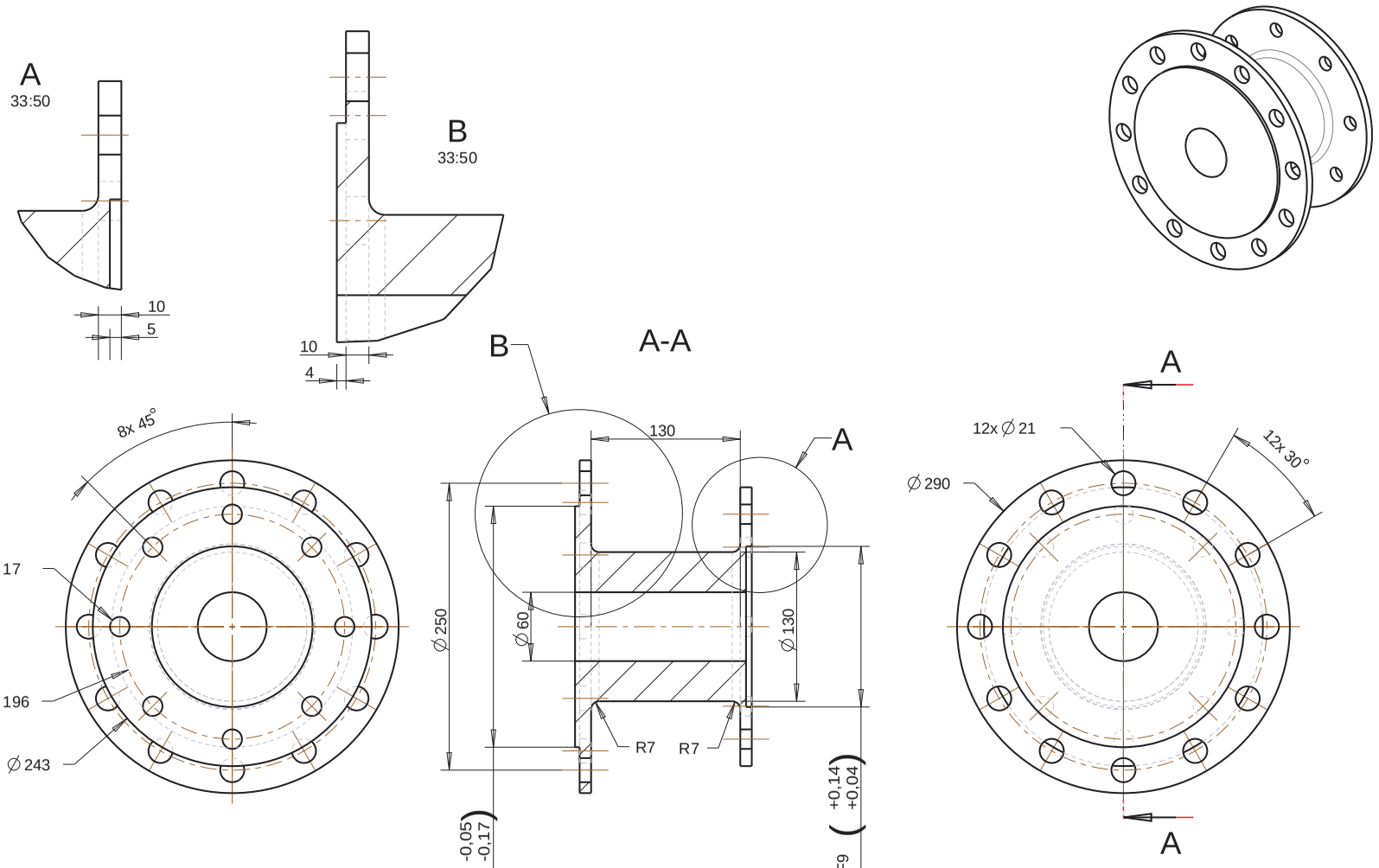

Adapter 3
Scale: 33:100
Ej toleranssatta mått: ±0.1 mm

Johan Karlsson, a188857
johan.karlsson.19@volvo.com